ISSN 0280–5316
ISRN LUTFD2/TFRT--5538--SE

Analysis of Static Nonlinearities Based on Integral Quadratic Constraints

Maria-Christina Laiou

(Imperial College of Science
Technology & Medicine
London, UK)

Department of Automatic Control
Lund Institute of Technology
September 1995

Department of Automatic Control
Lund Institute of Technology
P.O. Box 118
S-221 00 Lund Sweden

Document name
MASTER THESIS

Date of issue
September 1995

Document Number
ISRN LUTFD2/TFRT--5538--SE

Author(s)
Maria-Christina Laiou
of
Imperial College of Science, Technology & Medicine

Supervisor
Anders Rantzer and Ulf Jönsson

Sponsoring organisation

Title and subtitle
Analysis of Static Nonlinearities based on Integral Quadratic Constraints

Abstract

This thesis focuses on how to use Integral Quadratic Constraints (IQC's) for the stability analysis of feedback systems with static nonlinearities. A review of IQC's satisfied by nonlinearities commonly encountered in control systems is given first and then the LMI formulation of these IQC's is studied. The results are applied to three examples, which illustrate how our method works. The most important example concerns the stability and robustness analysis of a control system with a saturation, controlled by a PI controller with anti-windup. It becomes clear how easily the IQC's description of nonlinearities allows extension of the results to cases where more than one perturbation is present

Key words
Stability Analysis, Static Nonlinearities, Integral Quadratic Constraints (IQC), Linear Matrix Inequalities (LMI)

Classification system and/or index terms (if any)

Supplementary bibliographical information

ISSN and key title
0280–5316

ISBN

Language
English

Number of pages
76

Recipient's notes

Security classification

The report may be ordered from the Department of Automatic Control or borrowed through the University Library 2, Box 1010, S-221 03 Lund, Sweden, Fax +46 46 110019, Telex: 33248 lubbis lund.

Acknowledgements

The thesis has been carried out in the Technical University of Lund, Sweden, under an exchange programme with Imperial College of Science, Technology and Medicine, London. I would like to thank both Imperial College and the Technical University of Lund for giving me this opportunity.

I would also like to express my sincere thanks to my supervisors, Anders Rantzer and Ulf Jönsson for their help and support throughout the thesis.

Contents

Introduction

This thesis deals with the stability analysis of control systems with static nonlinearities and uncertainties using the method of Integral Quadratic Constraints (IQC's). The nominal system is supposed to be linear, time-invariant and stable. The perturbations are considered to be causal and bounded.

The motivation for this work originates from the fact that static nonlinearities are very commonly encountered in control systems. Amplifiers, actuators, sensors, motors, valves and electrical relays usually have characteristics that can be modeled by nonlinear functions such as saturations, relays, dead-zones, friction models. Consider for example the system shown in Figure 1, which could describe the system of a double tank with a PID controller and an anti-windup filter W. The saturation would in this case describe the characteristic function of a pump. Such systems can easily be transformed to the feedback system shown in Figure 2, to which the theory applies. In this system, Δ is a bounded nonlinearity, or in the general case a diagonal matrix whose elements are bounded nonlinearities or uncertainties.

The term *integral quadratic constraint* is used for an inequality describing constraints on a perturbation or an external signal. The constraint has the form of a weighted quadratic frequency integral.

IQC's have been present in the control literature for more than thirty years. Until the 60's the stability analysis of single-input/single-output systems like the one shown in Figure 0.2 was based on graphical criteria, such as the Popov criterion and the circle criterion, which often give conservative stability conditions. Later in the 60's, Zames and Falb introduced a more general class of multipliers which includes the above mentioned criteria. In the 70's, IQC's were used, and named so, by Yacubovich, to treat the stability problem for systems with more advanced nonlinearities. The usefulness of the above approaches was limited by the lack of appropriate software. The recent development of interior point methods for solving systems of *Linear*

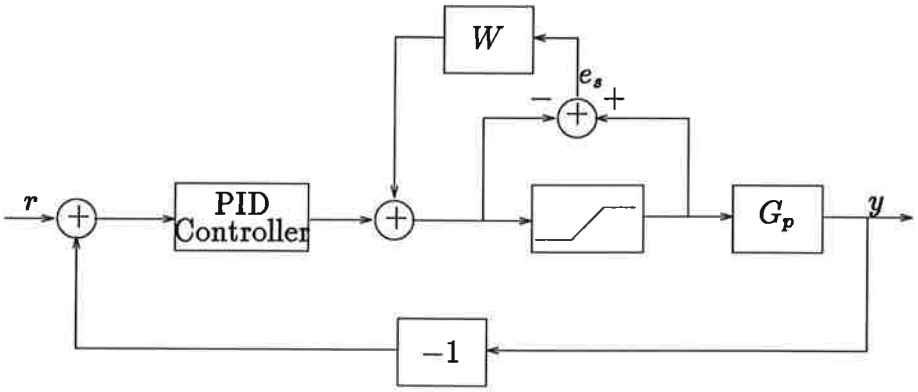

Figure 0.1: Control system with saturation and PID controller with anti-windup

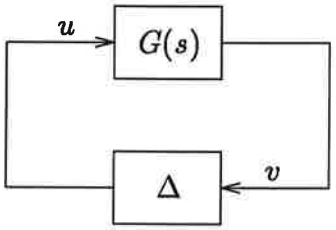

Figure 0.2: Feedback system

Matrix Inequalities (LMI's) has strongly improved the possibility to analyze complex systems using combinations of different IQC's. See [8], [10] and the references therein for more details.

The work of this thesis is based on the results given in [8] and [10]. A review of these results as well as some well known IQC's are given and a recently proved IQC concerning a friction model is considered. Particular emphasis is given on the formulation of the stability criteria in terms of LMI's. This is proved to be very useful, as the representation of IQC's in an LMI form allows recycling in other problems where the same type of nonlinearities appear.

More specifically, the thesis is structured as follows.

The first two chapters give some mathematical preliminaries and a short

review of the most essential results on the use of IQC's for stability analysis of feedback systems with static nonlinearities.

In Chapter 3 the IQC's concerning sector restricted nonlinearities, slope restricted nonlinearities and a friction model are presented. We also discuss a number of nonlinearities which are often found in practical applications and fall within the framework of the already studied IQC's.

Chapter 4 concentrates on the LMI formulation of the results presented in the previous chapters. The results given in [7] are first reviewed and then they are applied to the special case of slope restricted nonlinearities. Emphasis is given on the choice of multipliers for this type of nonlinearities and a method for selecting the appropriate ones is proposed.

In Chapter 5 the above theory is applied to three different examples. The two first are just theoretical. However, they illustrate very clearly the way that our method works, as well as the efficiency of the developed software. Example 3 is particularly interesting, as it applies our results to a practical system including a regulator with anti-windup. The case of a saturation is studied first. The results are then extended to the case of the simultaneous presence of a multiplicative uncertainty in the system's dynamics. It becomes clear how easily our method allows extension of the results to the case of several nonlinearities and uncertainties.

Two appendices are given in the end of the report. Appendix A includes the proofs of the theorems presented in Chapter 3. In Appendix B the Matlab programs that have been used for the necessary computations are listed.

Chapter 1

Notation and Mathematical Preliminaries

In this chapter the notation which will be used throughout the thesis, as well as some function spaces and mathematical results are given.

- $\mathbf{R}$ denotes the set of real numbers and $\mathbf{R}^{m\times n}$ the set of $m \times n$ matrices with elements in $\mathbf{R}$.
- M^T denotes the transpose of a matrix.
- M^* is the Hermitian conjugate of a complex matrix.
- $\mathbf{L}_2^m(-\infty,\infty)$ denotes the space of square integrable functions $(-\infty,\infty) \rightarrow \mathbf{R}^m$. For a function $f \in \mathbf{L}_2^m(-\infty,\infty)$ we define the L_2-norm as $\|f\|_2 = \left(\int_{-\infty}^{\infty} f^T(t)f(t)dt\right)^{1/2}$. $\mathbf{L}_2^m[0,\infty)$ can be viewed as a subspace of $\mathbf{L}_2^m(-\infty,\infty)$ with $f(t) = 0, \quad \text{for} \quad t < 0$. The L_2-norm of a function f in $\mathbf{L}_2^m[0,\infty)$ is defined as $\|f\|_2 = \left(\int_0^{\infty} f^T(t)f(t)dt\right)^{1/2}$.
- The *Fourier transform* of a signal $u(t) \in \mathbf{L}_2(-\infty,\infty)$ is defined as

$$\hat{u}(j\omega) = \mathcal{F}\{u(t)\} = \int_{-\infty}^{\infty} u(t)e^{-i\omega t}dt$$

- *Parseval's Theorem* : If $u, v \in \mathbf{L}_2^m(-\infty,\infty)$, then

$$\int_{-\infty}^{\infty} u^T(t)v(t)dt = \frac{1}{2\pi}\int_{-\infty}^{\infty} \hat{u}^*(j\omega)\hat{v}(j\omega)d\omega$$

- Introduce also the truncation operator P_T, which leaves a function unchanged on the interval $[0,T]$ and gives the value zero on $[T,\infty]$. *Causality* of an operator F means that $P_T F = P_T F P_T$.

- An operator $H : \mathbf{L}_2^m[0,\infty) \to \mathbf{L}_2^m(-\infty,\infty)$ is said to be bounded if the gain

$$\|H\| = \sup_{v \in \mathbf{L}_2^m} \frac{\|Hv\|_2}{\|v\|_2}$$

is finite. A bounded causal operator maps $\mathbf{L}_2[0,\infty]$ into itself.

- Let $\mathbf{RL}_\infty$ be the set of proper (bounded at infinity) rational functions with real coefficients and no poles on the imaginary axis. Any function $H \in \mathbf{RL}_\infty$ has a (not unique) realization $H(s) = C(sI - A)^{-1}B + D$, where $\det(A - j\omega I) \neq 0, \quad \forall \omega \in \mathbf{R}$.

- The subset of $\mathbf{RL}_\infty$ consisting of functions without poles in the closed right half plane is denoted $\mathbf{RH}_\infty$.

- The set of $m \times n$ matrices with elements in $\mathbf{RL}_\infty$ ($\mathbf{RH}_\infty$) will be denoted $\mathbf{RL}_\infty^{m\times n}$ ($\mathbf{RH}_\infty^{m\times n}$).

- $\mathbf{RL}_1$ denotes the set of strictly proper rational functions with real coefficients and no poles on the imaginary axis. Any $H \in \mathbf{RL}_1$ has a realization $H(s) = C(sI - A)^{-1}B$, where $\det(A - j\omega I) \neq 0, \quad \forall \omega \in \mathbf{R}$. Any $H \in \mathbf{RL}_1$ can be uniquely written as $H = H_c + H_{ac}$, where $H_c = C_c(sI - A_c)^{-1}B_c$ corresponds to a causal operator, i.e. $\mathrm{eig}(A_c) < 0$, and $H_{ac} = C_{ac}(sI - A_{ac})^{-1}B_{ac}$ corresponds to an anticausal operator, i.e. $\mathrm{eig}(A_{ac}) > 0$. The corresponding impulse response is defined as follows:

$$h(t) = \begin{cases} C_c e^{A_c t} B_c, & t > 0 \\ C_{ac} e^{A_{ac} t} B_{ac}, & t \leq 0. \end{cases}$$

- $H \in \mathbf{RL}_1$ can be viewed as an operator $\mathbf{L}_2[0,\infty) \longrightarrow \mathbf{L}_2(-\infty,\infty)$, defined as follows: If $v \in \mathbf{L}_2[0,\infty)$, then H maps v into

$$(h * v)(t) = \int_{-\infty}^{\infty} h(t)v(t-\tau)d\tau = \int_{-\infty}^{\infty} v(t)h(t-\tau)d\tau$$

The Fourier transform of the above quantity is given as follows

$$\mathcal{F}\{h * v\}(j\omega) = \mathcal{F}\{h\}(j\omega)\mathcal{F}\{v\}(j\omega)$$

- Let $H \in \mathbf{RL}_1$. The L_1 norm of its impulse response is defined as

$$\begin{aligned} \|h\|_1 &= \int_{-\infty}^{\infty} |h(t)|dt = \int_{-\infty}^{\infty} |Ce^{At}B|dt \\ &= \int_0^{\infty} |C_c e^{A_c t} B_c|dt + \int_{-\infty}^{0} |C_{ac} e^{A_{ac} t} B_{ac}|dt. \end{aligned}$$

Chapter 2

Stability Analysis based on IQC's

We will in this chapter review the most essential results on how to use Integral Quadratic Constraints (IQC:s) for stability analysis of feedback systems as the one shown in Figure 2.1, see [10] and [8] for more details.

Consider the feedback system shown in Figure 2.1. It is assumed that G is a stable linear causal time-invariant operator with transfer function $G(s)$ in $\mathbf{RH}_\infty^{m\times m}$. The perturbation Δ is a bounded causal operator from $\mathbf{L}_2^m[0,\infty)$ to $\mathbf{L}_2^m[0,\infty)$.

We assume that the feedback system in Figure 2.1 satisfies the following *well-posedness condition*

Definition 2.1 *The feedback system in Figure 2.1 is said to be well posed if for every $T \geq 0$, there exists a causal inverse of the operator $I - P_T G\Delta$.*

We will be concerned with input/output stability in the following sense:

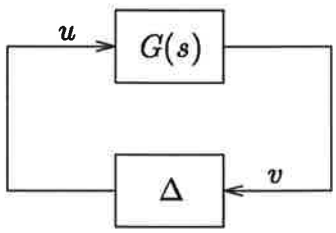

Figure 2.1: Feedback system

Definition 2.2 *The system of Figure 2.1 is input/output stable if it is well posed and $I - G\Delta$ has a bounded causal inverse, i.e. if there exists a $C > 0$, such that $\|(I - G\Delta)^{-1}\| \leq C$.*

The term IQC is defined as follows:

Definition 2.3 *Suppose $\Pi \in \mathbf{RH}_\infty^{m\times m}$. Δ is said to satisfy the IQC defined by Π, if*

$$\int_{-\infty}^{\infty} \begin{bmatrix} \hat{v}(j\omega) \\ \hat{u}(j\omega) \end{bmatrix}^* \Pi(j\omega) \begin{bmatrix} \hat{v}(j\omega) \\ \hat{u}(j\omega) \end{bmatrix} d\omega \geq 0$$

for any $\hat{v}$,$\hat{u}$ being the Fourier transforms of $v, u \in \boldsymbol{L}_2^m[0,\infty)$ with $u(t) = \Delta(v)(t)$.

A general stability theorem in terms of IQC's is stated below [10].

Theorem 2.1 *Let G be a linear causal operator with transfer function $G(s) \in \mathbf{RH}_\infty^{m\times m}$ and let Δ be a bounded causal operator on $\boldsymbol{L}_2^m[0,\infty)$. Assume that*

(i) for any $\tau \in [0,1]$, the interconnection of G and $\tau\Delta$ is well-posed,

(ii) for any $\tau \in [0,1]$, the IQC defined by Π is satisfied by $\tau\Delta$,

(iii) there exists $\varepsilon > 0$ such that

$$\begin{bmatrix} G(j\omega) \\ I \end{bmatrix}^* \Pi(j\omega) \begin{bmatrix} G(j\omega) \\ I \end{bmatrix} \leq -\varepsilon I, \quad \forall \omega \in [0,\infty]. \tag{2.1}$$

Then the feedback system in Figure 2.1 is input/output stable.

The basic idea for using these results in practice is as follows. First define a description of the perturbation Δ in terms of IQC's. The set of all Π functions which define valid IQC's for Δ is always convex. The stability analysis then consists of a search for a Π in this set such that (2.1) is satisfied. Normally we only know, or use, a subset of the Π–functions that describe Δ.

The following two properties are useful when defining an IQC description of a block diagonal perturbation Δ. Property 2 is particularly useful, as it shows that the description with IQC's easily allows extension of the stability analysis to the case of several uncertain or nonlinear blocks.

Property 1 If Δ satisfies the IQC's defined by $\Pi_1, \ldots, \Pi_n$, then Δ also satisfies the IQC defined by $\Pi = x_1\Pi_1 + \cdots + x_n\Pi_n$, where $x_1, \ldots, x_n$ are

nonnegative numbers. The more IQC's that can be verified for Δ, the more powerful analysis can be done.

Property 2 Assume that Δ has the block-diagonal structure $\Delta = \text{diag}\{\Delta_1, \ldots, \Delta_n\}$ and that Δ_i satisfies the IQC defined by Π_i. Then Δ satisfies the IQC defined by $\Pi = \text{daug}\{\Pi_1, \ldots, \Pi_n\}$, where the operation daug is defined below. For simplicity we give the result for the case $n = 2$, but this can be easily extended for the case

$$\Pi_i = \begin{bmatrix} \Pi_{i1} & \Pi_{i2} \\ \Pi_{i2}^* & \Pi_{i3} \end{bmatrix}, \quad i = 1, 2$$

where the block structures are consistent with the size of Δ_1 and Δ_2, then

$$\text{daug}\{\Pi_1, \Pi_2\} = \begin{bmatrix} \Pi_{11} & 0 & \Pi_{12} & 0 \\ 0 & \Pi_{21} & 0 & \Pi_{22} \\ \Pi_{12}^* & 0 & \Pi_{13} & 0 \\ 0 & \Pi_{22}^* & 0 & \Pi_{23} \end{bmatrix}$$

Chapter 3

IQC's for Different Types of Nonlinearities

This chapter presents a number of IQC's that describe nonlinearities which often appear in models of uncertain systems. More specifically, we give results concerning sector nonlinearities, slope restricted nonlinearities and a simple friction model. Examples of practical systems where the above nonlinearities can be found are discussed in the end of the chapter.

3.1 Memoryless Nonlinearity in a Sector

In this section we will discuss memoryless nonlinearities in the sector$[\alpha, \beta]$, which is defined as follows.

Definition 3.1 sector$[\alpha, \beta]$, $\alpha < \beta$, *denotes the class of memoryless nonlinearities* φ *which satisfy the following conditions*

$$\begin{aligned} \varphi(0,t) &= 0, \qquad \forall \quad t \in R^+ \\ \alpha v^2 \leq \varphi(v,t)v &\leq \beta v^2, \qquad \forall \quad v \in R, \quad t \in R^+ \end{aligned}$$

This definition is illustrated in Figure 3.1.

It is easy to verify the following two propositions, which define IQC's that describe sector bounded nonlinearities.

Proposition 3.1 *Consider a nonlinearity* $\varphi : R \times R^+ \to R$ *which belongs to* sector$[0, \infty)$. *Then* φ *satisfies the IQC defined by*

$$\Pi(j\omega) = \begin{bmatrix} 0 & I \\ I & 0 \end{bmatrix}$$

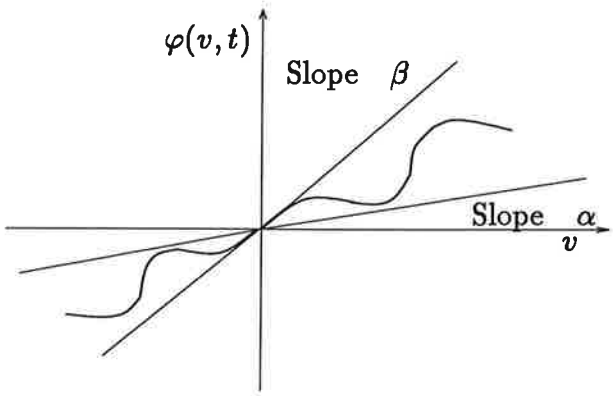

Figure 3.1: Nonlinearity in sector$[\alpha, \beta]$

The result of the above proposition can be generalized as it is shown in the following proposition, which gives the IQC corresponding to the circle criterion [15].

Proposition 3.2 *Consider a nonlinearity $\varphi : R \times R^+ \to R$ which belongs to sector$[\alpha, \beta]$. Then φ satisfies the IQC defined by*

$$\bar{\Pi}(j\omega) = \begin{bmatrix} -2\alpha\beta & \alpha+\beta \\ \alpha+\beta & -2 \end{bmatrix}$$

The proof of the above proposition is based on the fact that the nonlinearity $\varphi \in$ sector$[\alpha, \beta]$ can be transformed to a nonlinearity $\tilde{\varphi} \in$ sector$[0, \infty)$, for which Proposition 3.1 can be used. The transformation is achieved with the following two transformation matrices

$$T_1 = \begin{bmatrix} 1 & -\frac{1}{\beta-\alpha} \\ 0 & 1 \end{bmatrix}, \qquad T_2 = \begin{bmatrix} 1 & 0 \\ -\alpha & 1 \end{bmatrix}$$

It is easy to check that

$$\bar{\Pi}(j\omega) = (\beta - \alpha) T_2^T T_1^T \Pi(j\omega) T_1 T_2$$

where $\Pi(j\omega)$ is as in Proposition 3.1.

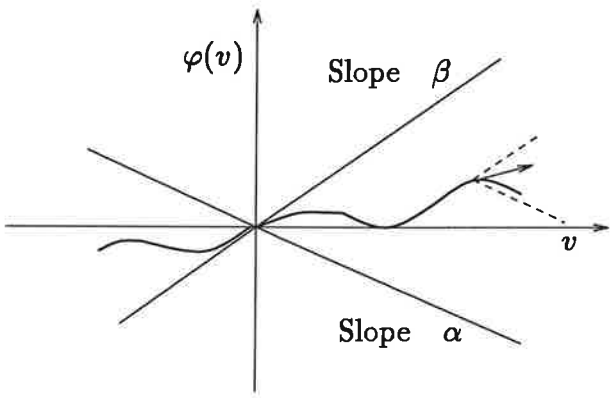

Figure 3.2: Nonlinearity with slope restricted in the sector $[\alpha, \beta]$

3.2 Slope Restricted Nonlinearities

This section deals with memoryless nonlinearities with slope in the interval $[\alpha, \beta]$. The class of these nonlinearities is defined as follows.

Definition 3.2 slope$[\alpha, \beta]$ *denotes the class of memoryless nonlinearities* φ *which have the following properties:*

(i) $\varphi(0) = 0$
(ii) there is a constant $k > 0$ *such that* $|\varphi(x)| \leq k|x|, \forall x$
(iii) φ *is odd*
(iv) $\alpha \leq \frac{\varphi(x_1)-\varphi(x_2)}{x_1-x_2} \leq \beta, \quad \forall x_1 \neq x_2$

where α, β *are constants with* $-\infty < \alpha < \beta < \infty$.

The above definition is illustrated in Figure 3.2. At every point, a tangent of $\varphi(v)$ lies in the sector $[\alpha, \beta]$.

The following theorem and corollary which define IQC's that describe slope restricted nonlinearities have been proven in [16]. The proofs are given in Appendix A.

Theorem 3.1 *Suppose that* φ *is a real-valued function on (-*∞*,*∞*) with the following properties:*

(i) $\varphi(0) = 0$
(ii) φ *is monotone nondecreasing, i.e.* $(x_1 - x_2)[\varphi(x_1) - \varphi(x_2)] \geq 0$
(iii) there is a constant $k > 0$ *such that* $|\varphi(x)| \leq k|x|, \forall x$
(iv) φ *is odd.*

Then φ satisfies the IQC defined by

$$\Pi(j\omega) = \begin{bmatrix} 0 & d + H(j\omega) \\ d + H^*(j\omega) & 0 \end{bmatrix}$$

where $H \in \boldsymbol{RL}_1$, i.e. $H(j\omega) = c_{ac}^T(j\omega I - A_{ac})^{-1}b_{ac} + c_c^T(j\omega I - A_c)^{-1}b_c$, and the L_1-norm of its impulse response is no larger than d, i.e.

$$\|h\|_1 = \int_{-\infty}^{\infty} |h(t)|dt = \int_{-\infty}^{0} \left|c_{ac}^T e^{A_{ac}t} b_{ac}\right| dt + \int_{0}^{\infty} \left|c_c^T e^{A_c t} b_c\right| dt \leq d$$

and d is a nonnegative constant.

In the above theorem, the indices c and ac denote causal and anti-causal components, respectively.

Remark If φ is not odd, the additional assumption that $h(t) \geq 0, \quad \forall t \in R$ is necessary.

The results of Theorem 3.1 can be generalized as it is shown in the following Corollary.

Corollary 3.1 *(Slope restricted nonlinearities) Suppose that, in addition to properties (i) and (iv) of Theorem 3.1, φ satisfies also the following condition*

$$\alpha \leq \frac{\varphi(x_1) - \varphi(x_2)}{x_1 - x_2} \leq \beta - \varepsilon, \quad \forall x_1 \neq x_2$$

where α and β are constants with $\alpha \leq \beta - \varepsilon$ and ε is a small positive number. Then φ satisfies the IQC defined by

$$\bar{\Pi}(j\omega) = \begin{bmatrix} 1 & 0 \\ -\alpha & 1 \end{bmatrix}^T \begin{bmatrix} 1 & -\frac{1}{\beta-\alpha} \\ 0 & 1 \end{bmatrix}^T \Pi(j\omega) \begin{bmatrix} 1 & -\frac{1}{\beta-\alpha} \\ 0 & 1 \end{bmatrix} \begin{bmatrix} 1 & 0 \\ -\alpha & 1 \end{bmatrix}$$

where $\Pi(j\omega)$ is as in Theorem 3.1.

3.3 A Friction Model

In this section we give an IQC which describes the nonlinearity shown in Figure 3.2. It is possible to use this nonlinearity as a model for friction. This is discussed in more detail in the next section. The following theorem gives the corresponding IQC.

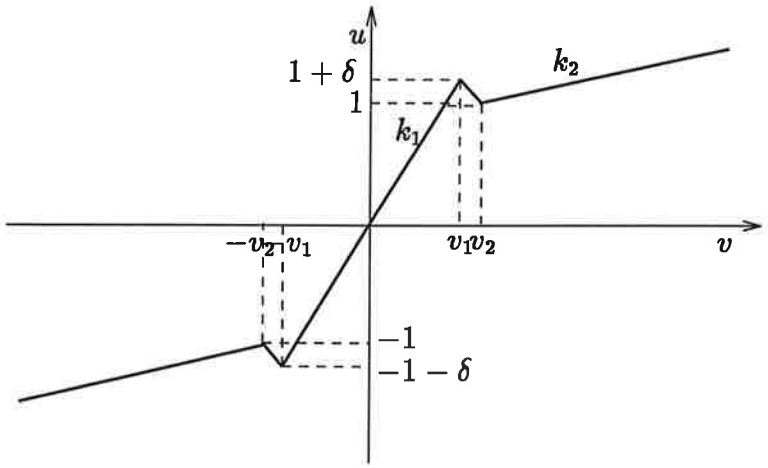

Figure 3.3: Stiction nonlinearity

Theorem 3.2 *Consider the nonlinearity φ shown in Figure 3.2. For $|v| \leq v_1$ φ has slope k_1 and for $|v| > v_2$ it has slope $k_2 < k_1$. The points v_1, v_2 are supposed to be known. Then φ satisfies the IQC defined by*

$$\bar{\Pi}(j\omega) = \begin{bmatrix} 1 & -\frac{1}{k_1} \\ -k_2 & 1 \end{bmatrix}^T \begin{bmatrix} 0 & 1 + H(j\omega) \\ 1 + H^*(j\omega) & 0 \end{bmatrix} \begin{bmatrix} 1 & -\frac{1}{k_1} \\ -k_2 & 1 \end{bmatrix}$$

where $H \in \boldsymbol{RL}_1$ and the L_1-norm of its impulse response is no larger than $\frac{1-k_2v_2}{(1+\delta)-k_2v_1}$.

The proof of the above theorem is given in Appendix A.

3.4 Common Nonlinearities in Control Systems

In this section we will present some nonlinearities which are often found in practical applications and can be treated in the same way as the nonlinearities which have been discussed in the previous sections.

3.4.1 Saturation

This kind of nonlinearity is shown in Figure 3.4 and can be defined as follows.

$$\text{sat}(v) = \begin{cases} kv, & |v| \leq v_0 \\ kv_0, & |v| > v_0 \end{cases}$$

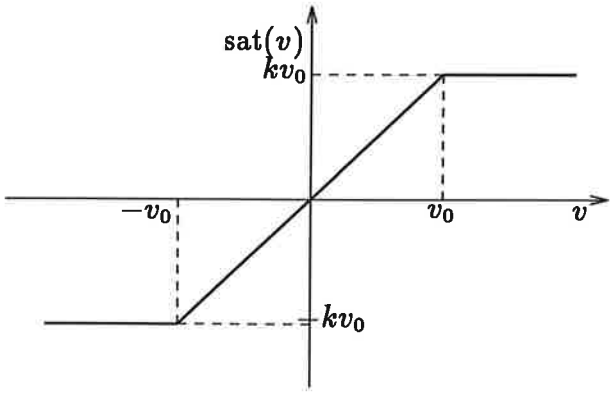

Figure 3.4: Saturation

The saturation is one of the most commonly encountered nonlinearities in control systems. It is usually caused by limits on component size, properties of materials and available power. It appears in amplifiers and actuators, which always have a finite working range.

In transistor amplifiers and magnetic amplifiers the output varies linearly with the input only for small amplitude inputs. When the input amplitude gets out of the linear range of the amplifier, the output changes very little and stays close to its maximum value, causing the saturation phenomenon.

Most actuators also have saturation characteristics. A typical example is a two-phase servo motor. Its output torque cannot increase infinitely and tends to saturate due to the properties of the magnetic material. Similar behaviour can be found in valve-controlled hydraulic servo motors, which are saturated by the maximum flow rate [12].

Since $\text{sat}(\cdot) \in \text{slope}[0, k]$, the IQC presented in section 3.2 can be used for the stability analysis of a feedback system including such a saturation.

3.4.2 Dead-Zone

A dead-zone is shown in Figure 3.5 and can be defined as follows.

$$dz(v) = \begin{cases} 0, & |v| \leq v_0 \\ v - v_0, & v > v_0 \\ v + v_0, & v < -v_0 \end{cases}$$

A dead-zone is quite often encountered in physical devices, where the

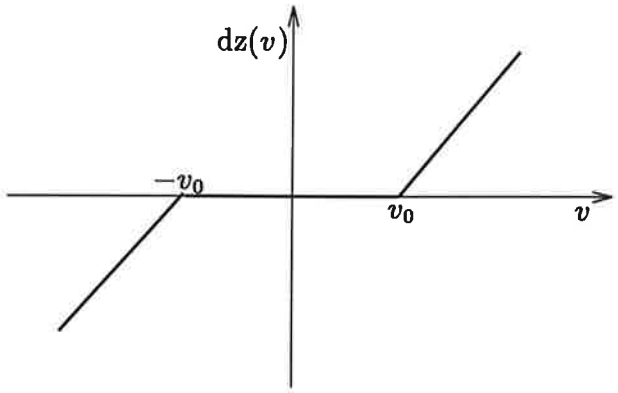

Figure 3.5: Dead Zone

output is zero until the amplitude of the input exceeds a certain value. Consider for example a d.c. motor. In linear system analysis it is assumed that rotation is possible for any value of the applied voltage, if the field current is maintained constant. In reality, due to friction, rotation occurs only if the torque provided by the motor is sufficiently large. This corresponds to a dead-zone for small voltage signals. Similar phenomena occur in valve-controlled pneumatic actuators and in hydraulic components [12].

A dead-zone describes also the relation between internal energy and temperature for materials which have a phase change. More specifically, the temperature, T, depends upon the internal energy, u, of the substance as follows.

$$T(u) = \begin{cases} C_l(u - L/2), & u > L/2 \quad \text{("unfrozen" substance)} \\ 0, & |u| \leq L/2 \quad \text{(phase change region)} \\ C_s(u + L/2), & u < L/2 \quad \text{("frozen" substance)} \end{cases}$$

where L is the "latent heat", C_l is the heat capacitance for the "unfrozen" region and C_s is the heat capacitance for the "frozen" region [3].

A dead zone can be considered as a nonlinearity which belongs to the class slope[0,k], where k is the slope in each specific case. Hence, the IQC presented in section 3.2 can be used.

3.4.3 Backlash

This nonlinearity is usually caused by the small gaps which exist in transmission mechanisms. In gear trains, there always exist small gaps between

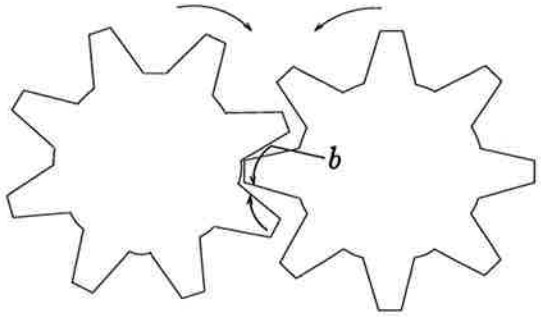

Figure 3.6: Backlash

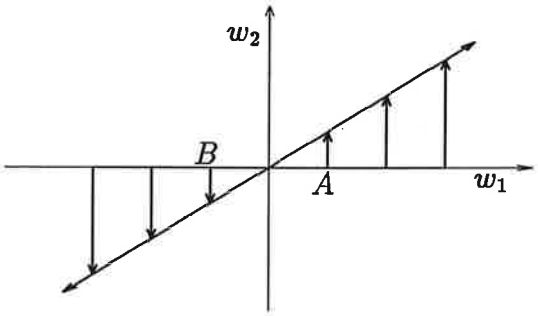

Figure 3.7: Backlash nonlinearity - Angular velocities of the gears in Figure 3.6

a pair of mating gears (Figure 3.6), due to errors in manufacturing and assembly. As a result, when the driving gear rotates a smaller angle than the gap b, the driven gear does not move at all. We make the assumption that, after contact has been established between the two gears, the driven gear follows the rotation of the driving gear [12]. This is the case, when there is a breaking torque acting on the driven gear which strives to make the angular speed of the driven gear zero, which is a quite ideal situation.

If w_1 and w_2 are the angular speeds of the driving and the driven gear, respectively, then their relation is described by the nonlinearity shown in Figure 3.7. When the driving gear begins moving, the speed w_2 of the driven gear will remain zero until a point A, where contact between the two gears is established. After this point, the angular velocities of the two gears will be practically the same. If at some point the driving gear changes direction of rotation, then w_2 will be zero as long as the angular distance between the two gears is less than b. After a point B, where contact is established, w_2

will depend linearly upon w_1.

According to the above analysis, the backlash nonlinearity belongs to the class sector$[0, k]$, where k is the slope of the linear parts of Figure 3.7. The corresponding IQC is the one presented in section 3.2.

3.4.4 Relay

This is an extreme case of saturation - the linearity range is zero and the slope in the linearity range is infinite. Important examples of relays include electrical relays, output torques of gas jets for spacecraft control and friction models in mechanical systems.

The relay nonlinearity can be approximated by a slope restricted nonlinearity, with $\alpha = 0$ and $\beta \to \infty$. Hence, Corollary 3.1 can be applied.

3.4.5 Friction

Consider the system shown in Figure 3.8, which is a model of a position controlled one degree of freedom rigid mass system with sliding friction. Simple or complicated systems may be considered with appropriate choices of $G_r(s)$, $G_1(s)$ and $G_2(s)$. This diagram can be manipulated to arrange all the linear elements as one block, leaving the nonlinear element as a second block, giving the block diagram of Figure 3.9 [1].

The nonlinearity $N(A)$ describes the relation between the friction and the velocity. A model of $N(A)$ is shown in Figure 3.10. It models static, kinetic and viscous friction and also a negative viscous friction at low velocity. Static friction is the force necessary to initiate motion from rest. In Figure 3.10, it is the friction corresponding to zero velocity. The kinetic friction is the friction component that is independent of the magnitude of the velocity. The viscous friction is proportional to velocity and is present in fluid lubricated junctions, such as machines lubricated by grease or oil. The sum of the kinetic and viscous friction corresponds to the linear part of the model in Figure 3.10. In many situations the force required to commence motion from rest is greater than that required to sustain motion. Detailed observation of friction suggests that the drop from static friction does not occur instantly but in the way shown in Figure 3.10. The region of negative viscous friction is that in which the friction force drops with increasing velocity [2].

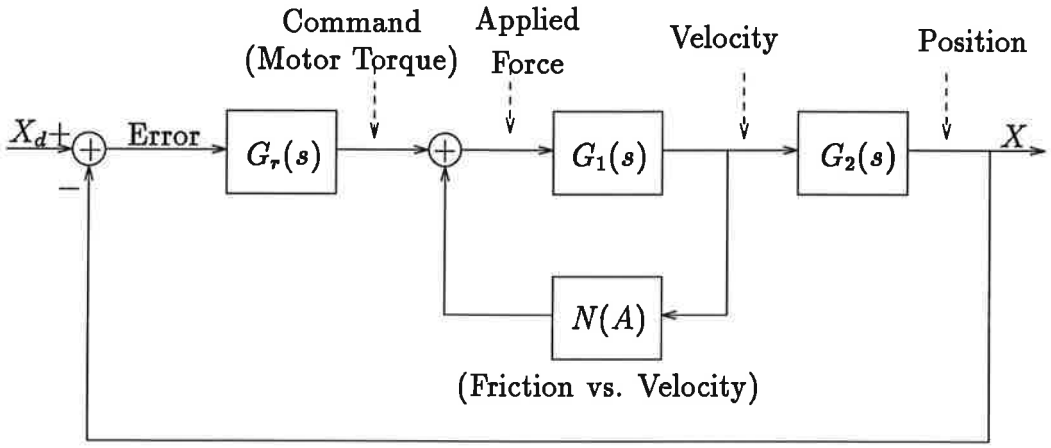

Figure 3.8: A single mass system with friction, friction modeled as a function of velocity.

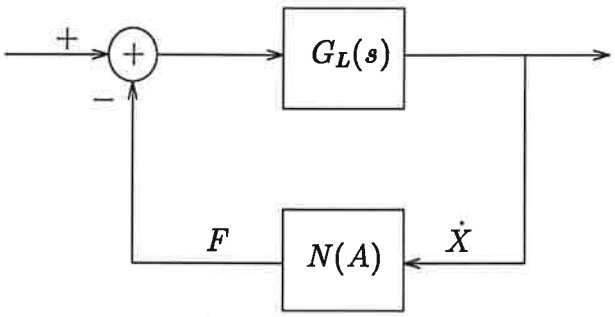

Figure 3.9: Simplified block diagram of the system shown in Figure 3.8

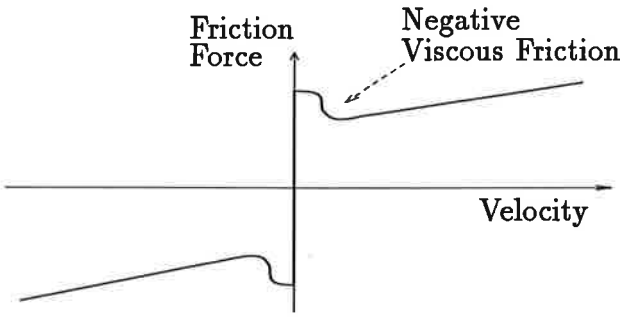

Figure 3.10: Negative viscous plus kinetic plus viscous friction model

The above friction model is like the one shown in Figure 3.3, when the slope k_1 tends to infinity. Hence, it will satisfy the IQC presented in section c3.3.

Another nonlinearity which looks exactly like the one discussed in section 3.3 can be found in models of tyres, see [6] for more details.

3.5 Summary

The IQC's that are satisfied by sector nonlinearities, slope restricted nonlinearities and a friction model have been presented in this chapter. Nonlinearities that are commonly encountered in control systems have also been discussed. From this discussion we see that the class of slope restricted nonlinearities covers a quite wide range of nonlinearities found in practical applications. The proposed friction model covers many different types of friction. In this model the slope k_1 is supposed to be finite, while in practice we often consider to have a nonzero friction for zero velocity. In some cases, this should not be a problem since k_1 is allowed to be arbitrarily large. This assumption though would probably not be able to treat any kind of friction.

Chapter 4

LMI Formulation

This chapter deals with the LMI formulation of results presented in previous chapters. A review of results on the LMI formulation of the stability criterion is given first. We then concentrate on the LMI formulation of the IQC satisfied by slope restricted nonlinearities. For this case, the choice of the appropriate multipliers is also discussed.

4.1 LMI Formulation of the Stability Criterion

In most cases the class of IQC's that describe the structure of a nonlinearity Δ is infinite. In [7] the following format has been suggested for the description of a class of IQC's

$$\Pi(j\omega) = \Psi(j\omega)^* M(\lambda)\Psi(j\omega) \tag{4.1}$$

where M is a fixed affine function of $\lambda \in R^n$ which takes values in the set of symmetric matrices in $R^{N\times N}$ and the range of λ is determined by the additional constraints

$$\Phi_k(j\omega)M(\lambda)\Phi_k(j\omega) \leq 0, \quad k = 1, \ldots, K \tag{4.2}$$

for all $\omega \in R$. $\Psi = \begin{bmatrix}\Psi^a & \Psi^b\end{bmatrix}$ is structured consistently with the structure of Δ. Hence, if Δ is an operator from $\mathbf{L}_2^l[0,\infty)$ to $\mathbf{L}_2^m[0,\infty)$, then $\Psi \in \mathbf{RL}_\infty^{N\times(l+m)}$, i.e. Ψ^a and Ψ^b have columns l and m, respectively. Let $\mathcal{P}(\Psi, \Phi, M)$ denote the set of matrix functions $\Pi(j\omega)$ defined as follows:

$$\mathcal{P}(\Psi, \Phi, M) = \{\Pi(j\omega) : \Psi(j\omega)^* M(\lambda)\Psi(j\omega) = \Pi(j\omega) \quad \text{for some } \lambda \in \Lambda\}$$

where

$$\Lambda = \{\lambda : \Phi_k(j\omega)M(\lambda)\Phi_k(j\omega) \leq 0, \quad k = 1, \ldots, K\}$$
$$\Phi = \{\Phi_1, \ldots, \Phi_k\}$$

The above description allows transformation of the stability condition by the Kalman-Yacubovich-Popov (KYP) Lemma into linear matrix inequalities.

In our applications we will only deal with constant matrices Φ_k. The following analysis is based on this assumption.

It has been mentioned in chapter 2 that a convenient way to obtain a description of an operator $\Delta = \text{diag}\{\Delta_1, \ldots, \Delta_N\}$ in terms of IQC's is to add and augment simple descriptions of the diagonal entries $\Delta_1, \ldots, \Delta_N$. It is easy to verify that this can be easily done when we use the above format. For the simple case of $N = 2$, addition and diagonal augmentation of the IQC classes defined by the sets $\mathcal{P}_1 = \mathcal{P}(\Psi_1, \Phi_1, M_1)$ and $\mathcal{P}_2 = \mathcal{P}(\Psi_2, \Phi_2, M_2)$ are achieved as follows

$$\mathcal{P}_1 + \mathcal{P}_2 = \mathcal{P}\left(\begin{bmatrix} \Psi_1 \\ \Psi_2 \end{bmatrix}, \left\{ \begin{bmatrix} \Phi_1 \\ 0 \end{bmatrix}, \begin{bmatrix} 0 \\ \Phi_2 \end{bmatrix} \right\}, \begin{bmatrix} M_1 & 0 \\ 0 & M_2 \end{bmatrix} \right)$$

and

$$\text{daug}(\mathcal{P}_1, \mathcal{P}_2) = \mathcal{P}\left(\Psi, \left\{ \begin{bmatrix} \Phi_1 \\ 0 \end{bmatrix}, \begin{bmatrix} 0 \\ \Phi_2 \end{bmatrix} \right\}, \begin{bmatrix} M_1 & 0 \\ 0 & M_2 \end{bmatrix} \right)$$

where

$$\Psi = \begin{bmatrix} \Psi_1^a & 0 & \Psi_1^b & 0 \\ 0 & \Psi_2^a & 0 & \Psi_2^b \end{bmatrix}$$

The above results can be easily extended to the case of $N > 2$.

Given a description of a nonlinearity Δ as in (4.1) and (4.2), the stability test corresponding to Theorem 2.1 can be stated as follows.

Feasibility Test
Find $\lambda \in R^n$ such that the following inequalities are satisfied

$$\begin{bmatrix} G(j\omega) \\ I \end{bmatrix}^* \Psi(j\omega)^* M(\lambda) \Psi(j\omega) \begin{bmatrix} G(j\omega) \\ I \end{bmatrix} < 0, \quad \forall \omega \in [0, \infty]$$

$$\Phi_k^* M(\lambda) \Phi_k \leq 0, \quad k = 1, \ldots, K$$

Assume that we have a realization

$$\Psi \begin{bmatrix} G \\ I \end{bmatrix} = C(sI - A)^{-1}B + D$$

where $\det(j\omega I - A) \neq 0, \quad \forall \omega \in R$. Application of the KYP Lemma as it is stated below gives the following LMI formulation of the Feasibility Test.

LMI Formulation for Feasibility Test
Find $\lambda \in R^n$ such that the following inequalities hold

$$\begin{bmatrix} A & B \\ I & 0 \\ C & D \end{bmatrix}^T \begin{bmatrix} 0 & P & 0 \\ P & 0 & 0 \\ 0 & 0 & M(\lambda) \end{bmatrix} \begin{bmatrix} A & B \\ I & 0 \\ C & D \end{bmatrix} < 0$$

$$\Phi_k^T M(\lambda) \Phi_k \leq 0, \quad k = 1, \ldots, K$$

where $P = P^T \in R^{n_a \times n_a}$ and n_a=dim(A).

Lemma 4.1 - *KYP [14]*
For the system $\Phi(s) = C(sI - A)^{-1}B + D$, where $det(j\omega I - A) \neq 0$, the following inequalities are equivalent. M is a symmetric matrix.
(i) $\Phi^*(j\omega) M \Phi(j\omega) < 0, \forall \quad \omega \in [0, \infty]$
(ii) There exists a matrix $P = P^T$ such that

$$\begin{bmatrix} A & B \\ I & 0 \\ C & D \end{bmatrix}^T \begin{bmatrix} 0 & P & 0 \\ P & 0 & 0 \\ 0 & 0 & M \end{bmatrix} \begin{bmatrix} A & B \\ I & 0 \\ C & D \end{bmatrix} < 0.$$

4.2 LMI Formulation for Slope Restricted Nonlinearities

It has already been proven that a nonlinearity φ having the properties stated in Theorem 1 satisfies the IQC defined by

$$\Pi(j\omega) = \begin{bmatrix} 0 & d + H(j\omega) \\ d + H^*(j\omega) & 0 \end{bmatrix} \tag{4.3}$$

where d is a nonnegative constant and $H \in \mathbf{RL}_1$ is strictly proper, with the L_1-norm of its impulse response no larger than d.

Introduce the "basis multipliers" $H_i \in \mathbf{RL}_1, \quad i = 1, \ldots, N$ and let

$$H = \sum_{i=1}^{N} x_i H_i \tag{4.4}$$

where x_i are real numbers.

The constraint on the L_1-norm of the impulse response of H will be replaced by the following one

$$\sum_{i=1}^{N} |x_i| \parallel h_i \parallel_1 \leq d \tag{4.5}$$

where $\|h_i\|_1$ is the L_1 norm of the basis multiplier H_i. Note that (4.5) is not equivalent to the constraint on the L_1 norm of h. It is in general a conservative estimate of the L_1 norm. This will be discussed in detail in the next subsection.

The relationship (4.5) is not linear in x_i, because of the absolute values appearing there. In order to get it in linear form, we introduce the positive and negative terms of x_i's, defined as follows

$$\begin{aligned} x_i^+ &= \max(x_i, 0) \\ x_i^- &= \max(-x_i, 0). \end{aligned}$$

It is then possible to write

$$\begin{aligned} x &= x^+ - x^- \\ |x| &= x^+ + x^-. \end{aligned}$$

Hence, relationships (4.3) and (4.5) can be written as follows

$$\Pi(j\omega) = \begin{bmatrix} 0 & d + \sum_{i=1}^{N} (x_i^+ - x_i^-) H_i(j\omega) \\ d + \sum_{i=1}^{N} (x_i^+ - x_i^-) H_i^*(j\omega) & 0 \end{bmatrix} \tag{4.6}$$

and

$$\sum_{i=1}^{N} (x_i^+ + x_i^-) \parallel H_i \parallel - d \leq 0 \tag{4.7}$$

where

$$d, x_i^+, x_i^- \geq 0, \quad i = 1 \ldots N. \tag{4.8}$$

Let λ correspond to d and $x_i^+, x_i^-, i = 1 \dots N$ and define the matrices

$$M(\lambda) = \begin{bmatrix} \mathbf{0}_{(2N+1)\times(2N+1)} & D(\lambda) \\ D(\lambda) & \mathbf{0}_{(2N+1)\times(2N+1)} \end{bmatrix} \tag{4.9}$$

where $D(\lambda) = \text{Diag}\{d, x_1^+, x_1^-, \dots, x_N^+, x_N^-\}$ and

$$\Psi(j\omega) = \begin{bmatrix} 0 & 1 \\ 0 & H_1 \\ 0 & -H_1 \\ \vdots & \vdots \\ 0 & H_N \\ 0 & -H_N \\ 1 & 0 \\ 1 & 0 \\ 1 & 0 \\ \vdots & \vdots \\ 1 & 0 \\ 1 & 0 \end{bmatrix}, \Phi_1(j\omega) = \begin{bmatrix} -1 \\ \| H_1 \| \\ \| H_1 \| \\ \vdots \\ \| H_N \| \\ \| H_N \| \\ 1 \\ 1 \\ 1 \\ \vdots \\ 1 \\ 1 \end{bmatrix}, \Phi_2(j\omega) = \begin{bmatrix} \mathbf{I}_{2N+1} \\ -\mathbf{I}_{2N+1} \end{bmatrix} \tag{4.10}$$

where $\mathbf{I}_{2N+1}$ is the $(2N+1) \times (2N+1)$ identity matrix. It is easy to see that the matrix $\Pi(j\omega)$ of equation (4.6) can be written as

$$\Pi(j\omega) = \Psi(j\omega)^* M(\lambda) \Psi(j\omega)$$

and that the inequalities (4.7) and (4.8) are respectively equivalent to the following inequalities

$$\Phi_1(j\omega)^* M(\lambda) \Phi_1(j\omega) \leq 0 \tag{4.11}$$

$$\Phi_2(j\omega)^* M(\lambda) \Phi_2(j\omega) \leq 0 \tag{4.12}$$

In the case of a nonlinearity φ satisfying the conditions of Corollary 3.1, i.e. a nonlinearity satisfying the IQC defined by

$$\bar{\Pi}(j\omega) = \begin{bmatrix} 1 & 0 \\ -\alpha & 1 \end{bmatrix}^T \begin{bmatrix} 1 & -\frac{1}{\beta-\alpha} \\ 0 & 1 \end{bmatrix}^T \Pi(j\omega) \begin{bmatrix} 1 & -\frac{1}{\beta-\alpha} \\ 0 & 1 \end{bmatrix} \begin{bmatrix} 1 & 0 \\ -\alpha & 1 \end{bmatrix}$$

the same analysis can be applied. The inequalities (4.7) and (4.8) hold also in this case and the matrices $M(\lambda), \Psi(j\omega), \Phi_1(j\omega)$ and $\Phi_2(j\omega)$ are still defined

as in equations (4.9) and (4.10). Hence, the inequalities (4.11) and (4.12) remain the same, while the matrix $\bar{\Pi}(j\omega)$ can be written as

$$\bar{\Pi}(j\omega) = \bar{\Psi}(j\omega)^* M(\lambda) \bar{\Psi}(j\omega) \tag{4.13}$$

where

$$\bar{\Psi}(j\omega) = \Psi(j\omega) \begin{bmatrix} 1 & -\frac{1}{\beta-\alpha} \\ 0 & 1 \end{bmatrix} \begin{bmatrix} 1 & 0 \\ -\alpha & 1 \end{bmatrix} \tag{4.14}$$

and $\Psi(j\omega)$ is given in (4.10).

A Matlab function which does the above LMI formulation for a given set of multipliers has been written. This is called slopeNL.m and a list of it is given in Appendix B.

4.2.1 Choice of Multipliers

The previous discussion implies that $H \in \mathbf{L}_1(-\infty, \infty)$. Here we are going to decompose H into a sum of causal and anti-causal components.

The space $\mathbf{L}_1(-\infty, \infty)$ can be decomposed as $\mathbf{L}_1(-\infty, \infty) = \mathbf{L}_1(-\infty, 0] \oplus \mathbf{L}_1[0, \infty)$, i.e. for every $h(\cdot) \in \mathbf{L}_1(-\infty, \infty)$, we can write $h(t) = h^+(t) + h^-(t)$ where

$$h^+(t) = \begin{cases} h(t), & t \geq 0 \\ 0, & t < 0 \end{cases} \qquad h^-(t) = \begin{cases} 0, & t > 0 \\ h(t), & t \leq 0 \end{cases}$$

The following lemma [5] allows us to approximate $h^+(t)$ and $h^-(t)$ by a finite sum.

Lemma 4.2 *If $f(t) \in \mathbf{L}_1[0, \infty)$, then for every $\varepsilon > 0$ there exists a vector $(x_0, x_1, \ldots, x_N) \in R^{(N+1)}$ such that*

$$\int_0^\infty \left| f(t) - \sum_{i=0}^{N} x_i t^{(i+\alpha)} e^{-t} \right| dt < \varepsilon$$

where $\alpha > -1$.

Replacing t by -t, the same result also holds for $\mathbf{L}_1(-\infty, 0]$. Instead of the factor e^{-t} we can, without any loss, use e^{-kt}, which simply introduces a

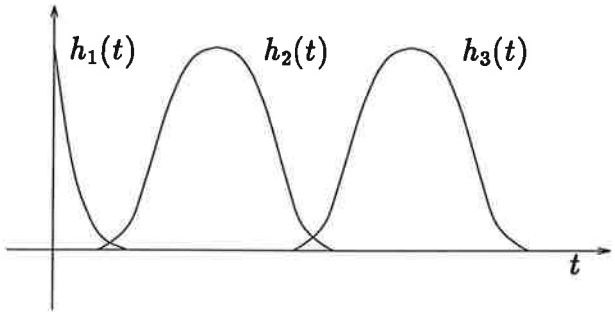

Figure 4.1: "Orthogonal" basis multipliers

time scaling. By choosing $\alpha = 0$, we obtain the following basis for the approximation:

$$h_i^+(t) = \begin{cases} t^i e^{-kt}, & t \geq 0 \\ 0, & t < 0 \end{cases} \qquad h_i^-(t) = \begin{cases} 0, & t > 0 \\ t^i e^{kt}, & t \leq 0 \end{cases}$$

Hence, an Nth order approximation of an $\mathbf{L}_1$ function $h(t)$ is given as follows

$$h(t) = \sum_{i=0}^{N} \left[a_i h_i^+(t) + b_i h_i^-(t) \right]$$

Note that for any values of i and k, the Laplace transform of $h(t)$ will be a rational function.

It should be mentioned here that with such a choice of basis multipliers the constraint on the $\mathbf{L}_1$ norm of the multiplier is usually conservative. It would be possible to avoid this conservativity by choosing the basis multipliers $h_i(t)$ as "orthogonal" functions in $\mathbf{L}_1$. This means that the $h_i(t)$ should be defined over different time intervals as shown in Figure 4.1. There is however a problem with this approach. The basis multipliers $h_i(t)$ must be linear combinations of exponential functions. This implies that the multipliers h_2 and h_3 in Figure 4.1 will be of high order, which would lead to complicated LMI computations.

In many cases it is sufficient to find the break frequencies in the Bode plot of the system transfer function $G(s)$, in order to decide about the basis multipliers that should be used. If for example the break frequencies are ω_1 and ω_2, then the set of multipliers

$$\mathcal{M} = \{e^{\omega_1 t}, e^{-\omega_1 t}, e^{\omega_2 t}, e^{-\omega_2 t}, \ldots, t^N e^{\omega_1 t}, t^N e^{-\omega_1 t}, t^N e^{\omega_2 t}, t^N e^{-\omega_2 t}\} \quad (4.15)$$

where N is the order of the approximation, can usually assure stability of the feedback loop. However, in most cases just a subset of $\mathcal{M}$ is enough for proving stability. Hence, by using all the elements of $\mathcal{M}$ we just introduce unnecessary and time-consuming computations. This can be avoided by careful inspection of the Nyquist and Bode plots of the system appearing in the stability condition. From these plots we can predict the frequencies over which the multiplier should be "active", as well as whether we should use a causal or an anti-causal multiplier. Useful information can also be obtained from a plot that shows how the largest eigenvalue corresponding to the inequalities of the feasibility test (see section 4.1) varies with frequency. The frequencies where there is a positive eigenvalue give us an indication of the frequencies over which the multiplier should act upon the system. Of course, this implies that more than one iterations of the Matlab program are normally necessary for finding the appropriate multiplier.

Usually more than one multiplier assures stability. In these cases, we prefer the simplest multiplier, or the one which allows better performance results.

It should finally be mentioned that in some cases it has not been possible to prove stability by using the set of multipliers given in (4.15). It is not clear if this has happened because this way of selecting basis multipliers is not correct or because the order N of the approximation that has been chosen was not large enough. It is quite probable that the reason was the not right choice of N, but this cannot be checked easily, as after some point the computations become very complicated and slow. However, even for these cases, it has been possible to find a suitable multiplier by following the above described method based on the Nyquist and Bode plots.

4.3 Summary

The LMI formulation of the IQC results presented in the previous chapters has been discussed here. The chapter focuses on the LMI formulation of the IQC satisfied by slope restricted nonlinearities. The choice of appropriate multipliers for this kind of nonlinearities has been discussed and a new method for selecting them has been proposed. The same problem is also studied in [5]. The efficiency of the method suggested here is illustrated in the next chapter, where the above theory is applied to specific examples.

Chapter 5

Examples

We will in this chapter apply the previously discussed theory to specific examples. The first two examples are theoretical and they illustrate the applicability of the theory and the efficiency of the developed software. The third example is practical and it offers a good insight on how our results can be used in practice for the stability analysis of systems with nonlinearities and uncertainties.

For the first two examples consider the system shown in Figure 5.1. The minus sign in the system transfer function $G(s)$ makes the closed loop system equivalent to a closed loop with negative feedback. This will be useful later for comparing our results with other already existing ones.

According to Corollary 3.1, a nonlinearity φ having the properties mentioned in Corollary 3.1 satisfies the IQC defined by

$$\bar{\Pi}(j\omega) = T_2^T T_1^T \Pi(j\omega) T_1 T_2$$

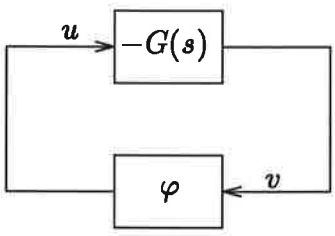

Figure 5.1: Perturbation in negative feedback form

where

$$\Pi(j\omega) = \begin{bmatrix} 0 & d + H(j\omega) \\ d + H^*(j\omega) & 0 \end{bmatrix}, \quad T_1 = \begin{bmatrix} 1 & -\frac{1}{\beta-\alpha} \\ 0 & 1 \end{bmatrix}, \quad T_2 = \begin{bmatrix} 1 & 0 \\ -\alpha & 1 \end{bmatrix},$$

d is a nonnegative constant, $H \in \mathbf{RL}_1$ is strictly proper, and the L_1-norm of its impulse response is no larger than d.

The stability criterion can then be written as follows:

$$\begin{bmatrix} -G \\ I \end{bmatrix}^* \bar{\Pi}(j\omega) \begin{bmatrix} -G \\ I \end{bmatrix} > 0, \quad \forall \omega \in [0, \infty].$$

Applying the appropriate transformations to the nonlinearity φ and the forward system $-G(s)$ (see Figure 5.2), the above inequality is equivalent to the following one:

$$\begin{bmatrix} \hat{G}(j\omega) \\ I \end{bmatrix}^* \Pi(j\omega) \begin{bmatrix} \hat{G}(j\omega) \\ I \end{bmatrix} < 0, \quad \forall \omega \in [0, \infty]$$

i.e.

$$\begin{bmatrix} \hat{G}(j\omega) \\ I \end{bmatrix}^* \begin{bmatrix} 0 & d + H(j\omega) \\ d + H^*(j\omega) & 0 \end{bmatrix} \begin{bmatrix} \hat{G}(j\omega) \\ I \end{bmatrix} < 0, \quad \forall \omega \in [0, \infty]$$

where

$$\hat{G} = \tilde{G} - \frac{1}{\beta - \alpha} \qquad \text{and} \qquad \tilde{G} = \frac{-G}{1 + \alpha G}.$$

Hence, the stability analysis problem of the feedback system shown in Figure 5.1 is equivalent to the following problem:

Find a multiplier H such that

$$Re\left[\hat{G}(j\omega)Z(j\omega)\right] < 0, \quad \forall \omega \in [0, \infty]$$

$$\text{where} \qquad Z(j\omega) = d + H^*(j\omega) = d + \sum_{i=1}^{N} x_i H_i^*(j\omega)$$

and $H_i(j\omega)$ are the basis multipliers.

The above theory has been applied to the following two examples which have been taken from [5], [13].

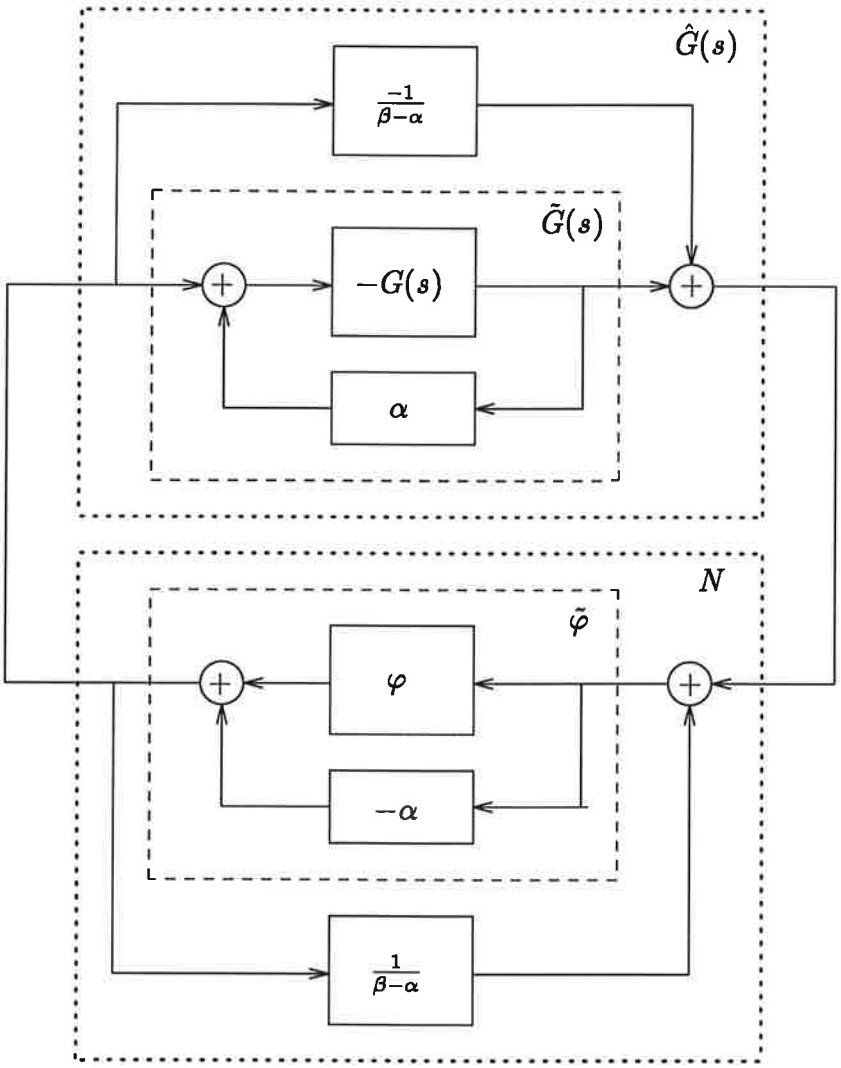

Figure 5.2: Transformed closed loop system

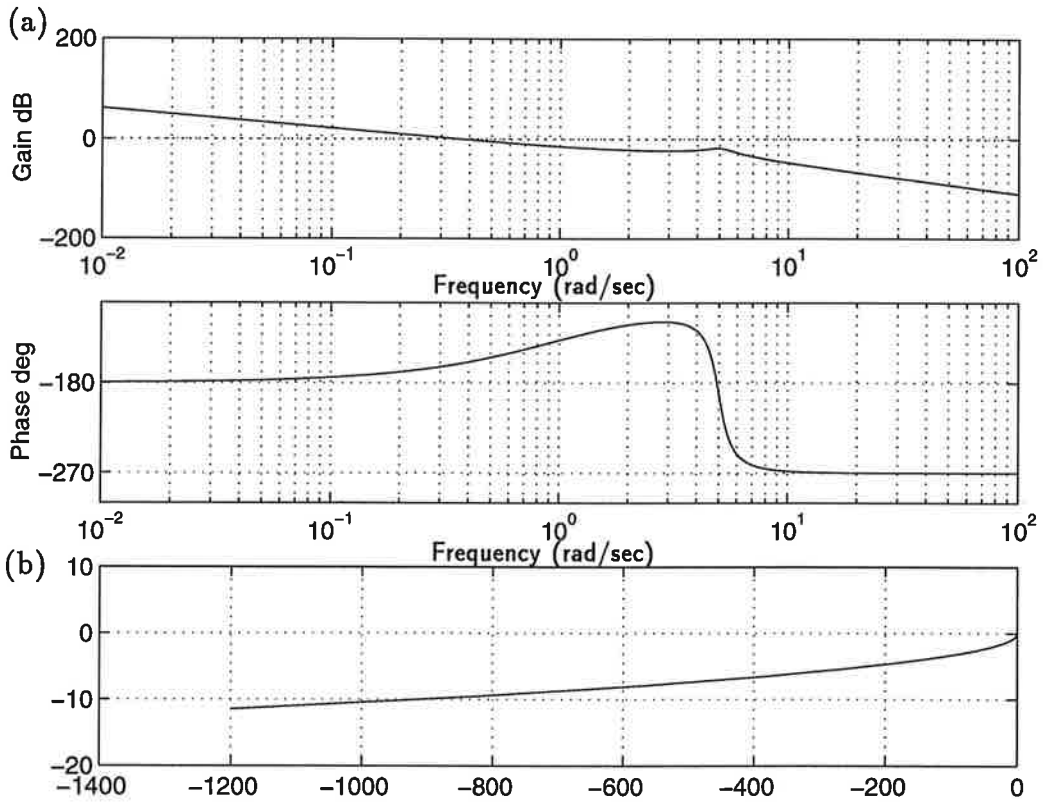

Figure 5.3: Example 1: (a) Bode plot of the transfer function $G(s)$ (b) Nyquist plot of the transfer function $G(s)$

5.1 Example 1

Let the system transfer function be

$$G(s) = \frac{3(s+1)}{s^2(s^2+s+25)}$$

Its Bode and Nyquist plots are shown in Figures 5.3(a) and (b), respectively.

We assume that an odd monotone nonlinearity $\varphi \in \text{slope}[1, \beta]$ is applied to the system in the way shown in Figure 5.1. Our goal is to find a bound for β that guaranties stability.

It should be mentioned that the fact that the system $G(s)$ is not stable (it has a double pole at s=0) does not cause any problems to the application of the theory, since the sector $[1, \beta]$ does not include zero. We assume that

$\alpha = 1$ is chosen so that the system $\tilde{G}(s)$, obtained after the first transformation shown in Figure 5.2 has been applied, is exponentially stable. This is necessary for stability. In our case, the system $\tilde{G}(s)$ is indeed stable. Its poles are $-0.4416 + 4.9579j, -0.4416 - 4.9579j, -0.0584 + 0.3430j$ and $-0.0584 - 0.3430j$, which lie in the left half plane.

The size of β cannot be larger than the Nyquist gain for $G(s)$, which corresponds to destabilization by a linear feedback element. The Nyquist gain is found to be $\beta_{max} = 8$. This conclusion can be drawn from Figure 5.4(a) where the Nyquist plot of the system $\tilde{G}(s)$, i.e. the closed loop system with forward transfer function $-G(s)$ and positive feedback gain $\alpha = 1$, has been plotted. It should be mentioned here that, since we use positive feedback, the critical point for the Nyquist criterion is the point (1,0). From the plot it is shown that the gain margin for the system $\tilde{G}(s)$ is 7, which gives an overall gain margin $\beta_{max} = 1 + 7 = 8$ for the system $G(s)$.

Figure 5.4(b) shows the Nyquist plot of the system $\hat{G}(s)$ which is obtained after both transformations have been applied to the original system $G(s)$. Figure 5.5 shows the Bode plot of the system $\hat{G}(s)$.

From the Bode plot in Figure 5.5 it is easy to find that the frequencies which correspond to $Re[\hat{G}(j\omega)] \geq 0$ are the frequencies in the interval [0.38, 0.93](rad/sec). Hence, in order for the stability condition to be satisfied, over this range of frequencies the multiplier should be able to add phase adequate to bring all the corresponding points of the Nyquist plot to the left half plane. More specifically, the multiplier $H(j\omega)$ should be such that the quantity $Z(j\omega) = d + xH^*(j\omega)$ adds positive phase to the system $\hat{G}(j\omega)$ over the frequencies [0.38, 0.93](rad/sec). Hence, we can expect that the multiplier will be "active" at frequencies between 0.1 rad/sec and 1 rad/sec.

LMI computations with several combinations of basis multipliers of the form $t^k e^{\lambda t}$ have been carried out. The objective was to find the multiplier which provides the largest stability bound, i.e. it satisfies the stability condition for the maximum upper bound β. Just by using one basis multiplier, namely the $h_1(t) = te^t$, $t > 0$, we can obtain an upper bound of β of 7.9999, which can be considered as a good approximation of the maximum Nyquist gain $\beta_{max} = 8$. The following analysis is based on the use of this basis multiplier.

According to (5.1), the multiplier which finally appears in the stability

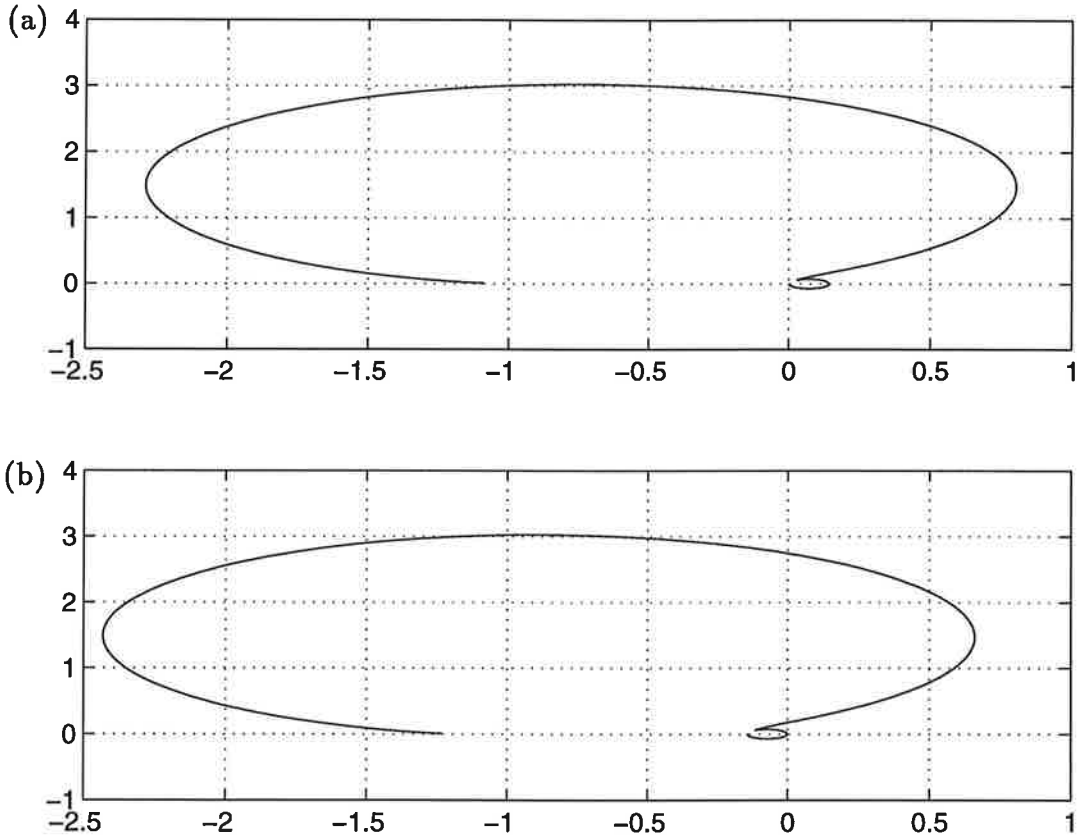

Figure 5.4: Example 1: (a) Nyquist plot of the transfer function $\tilde{G}(s)$ (b) Nyquist plot of the transformed forward system $\hat{G}(s)$

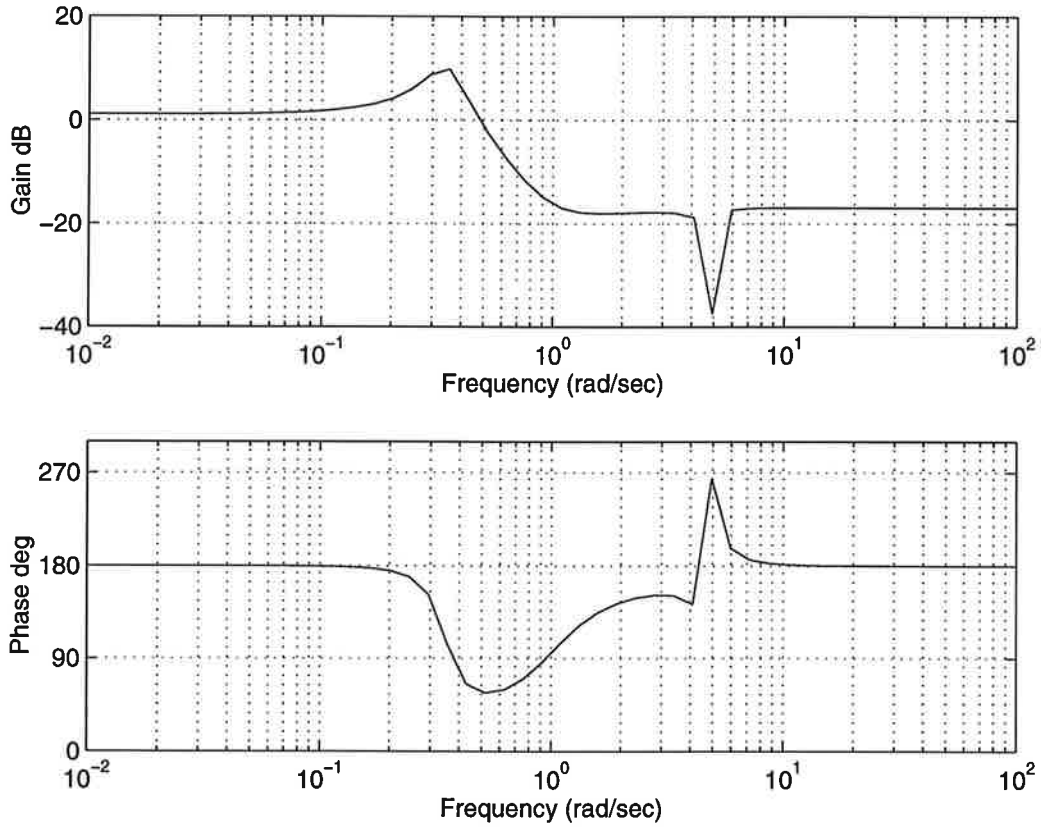

Figure 5.5: Example 1: Bode plot of the transformed forward system $\hat{G}(s)$

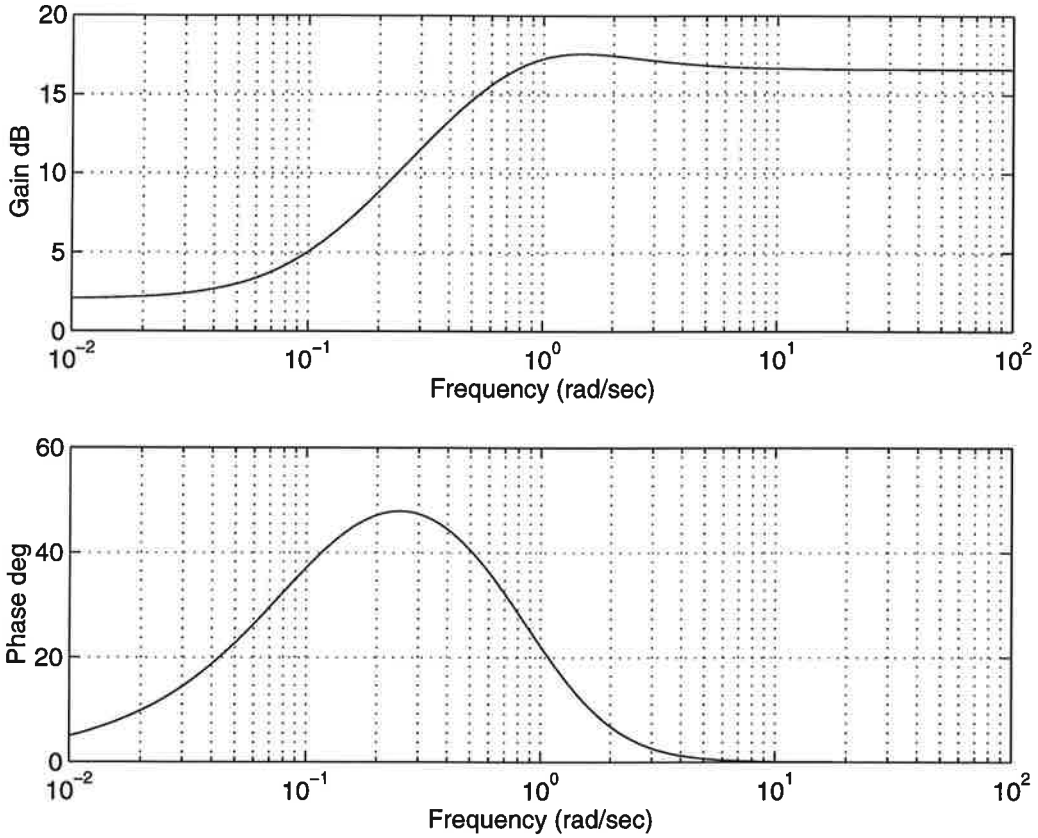

Figure 5.6: Example 1: Bode plot of $Z(j\omega) = d + x_1 H_1^*(j\omega)$. $H_1(j\omega) = 1/(j\omega - 1)^2$ is the Fourier transform of the basis multiplier $h_1(t) = te^t$

condition has the form

$$Z(j\omega) = d + x_1 H_1^*(j\omega)$$

where $H_1^*(j\omega) = 1/(s+1)^2$ is the complex conjugate of the Laplace transform of the basis multiplier $h_1(t)$ and d and x_1 are constants, see section 4.2, the values of which are found using LMI-Lab. The Bode plot of $Z(j\omega)$ is shown in Figure 5.6.

Comparing Figures 5.5 and 5.6, we see that at every frequency in the interval [0.38, 0.93](rad/sec) the phase of the multiplier is adequate to transfer the corresponding point of the Nyquist diagram of $\hat{G}(j\omega)$ to the left half plane. In addition, at every other frequency its phase is small enough to keep the corresponding points of the Nyquist plot at the left half plane. Hence, the stability condition will be satisfied for every $\omega \in [0, \infty]$. This is clearly

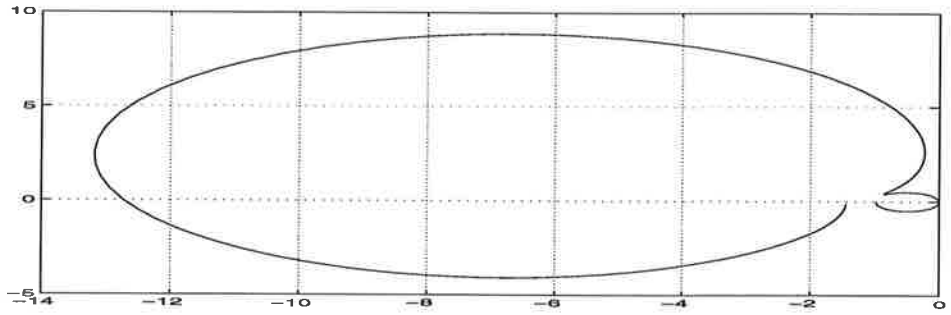

Figure 5.7: Example 1: Nyquist plot of the product of $\hat{G}(s)$ and $Z(j\omega)$

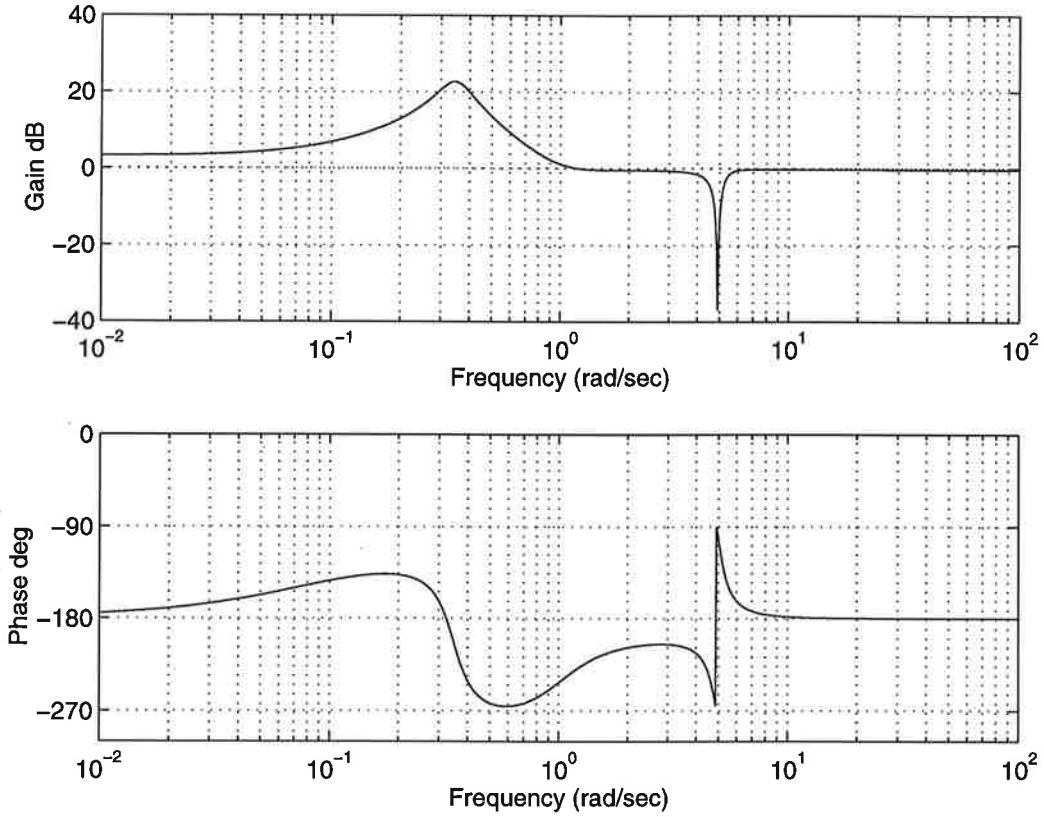

Figure 5.8: Example 1: Bode plot of the product of $\hat{G}(s)$ and $Z(j\omega)$

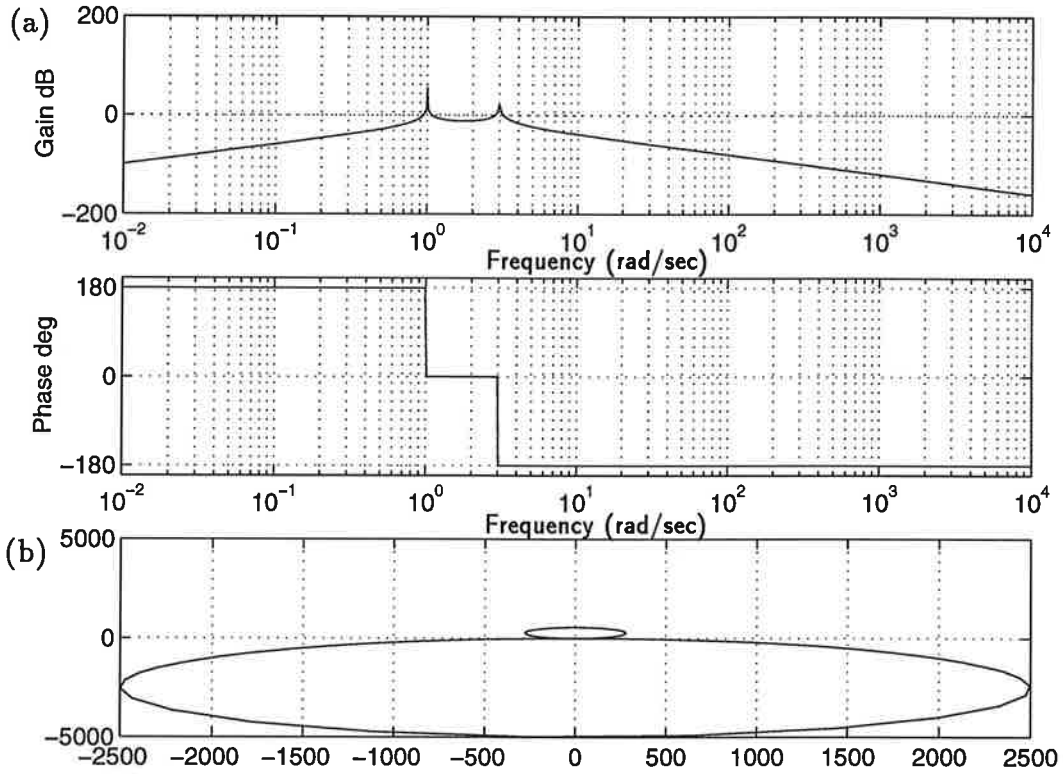

Figure 5.9: Example 2: (a) Bode plot of the transfer function $G(s)$ (b) Nyquist plot of the transfer function $G(s)$

shown in Figures 5.7 and 5.8 where the Nyquist and Bode plots of the product of $\hat{G}(j\omega)$ and $Z(j\omega)$ have been plotted. The Nyquist plot lies completely in the open left half plane and the phase in the Bode diagram is always in the interval $[-90^o, -270^o]$.

5.2 Example 2

Let the system transfer function be

$$\frac{s^2}{(s^2+1)(s^2+9)+10^{-4}(3s^3+21s)}$$

Its Bode and Nyquist plots are shown in Figures 5.9(a) and (b), respectively.

We assume that an odd monotone nonlinearity $\varphi \in$ slope $[0, \beta]$ is applied to the system in the way shown in Figure 5.1. Since $\alpha = 0$, only the second

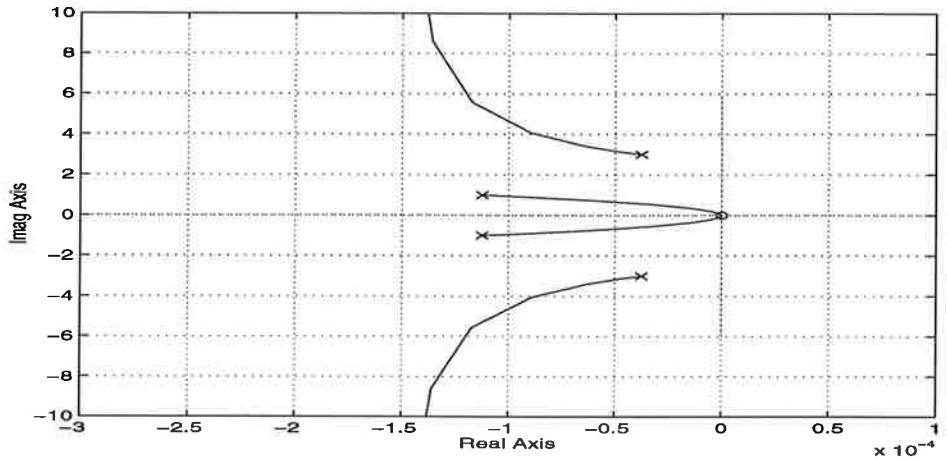

Figure 5.10: Example 2: Root locus of the closed loop system

transformation is needed. Hence, the transformed closed loop system will have the form shown in Figure 5.2, if the feedback loops with gains $\pm\alpha$ are omitted and the gains $\pm 1/(\beta - \alpha)$ are substituted with $\pm 1/\beta$.

The upper bound β cannot be larger than the Nyquist gain for $G(s)$, which corresponds to a linear feedback element. From Figure 5.9(b) it can be seen that, no matter how large the gain becomes, the Nyquist plot will never encircle the point (-1,0). Hence, the Nyquist gain for the system $G(s)$ will be ∞. This is shown more clearly in Figure 5.10, where the root locus of the function $G(s)$ has been plotted. The poles of the closed loop system with gain feedback lie always in the left half plane, although they are very close to the imaginary axis. Hence, the closed loop system will remain stable for infinitely large values of the linear feedback gain.

In Figure 5.11 the Nyquist plot of the system $\hat{G}(s) = -G(s) - \frac{1}{\beta}$, obtained after the transformation has been applied to the original system $G(s)$, is shown.

LMI computations with several combinations of basis multipliers of the form $t^k e^{\lambda t}$ have been carried out. As in Example 1, the objective was to find the multiplier which provides the largest stability bound, i.e. it satisfies the stability condition for the maximum upper bound β. Using the basis multiplier $h_1(t) = e^{10t}$, we can obtain an upper bound of β of 1.43 10^{-3}. This is higher than the one obtained in [5], which is an indication that our mul-

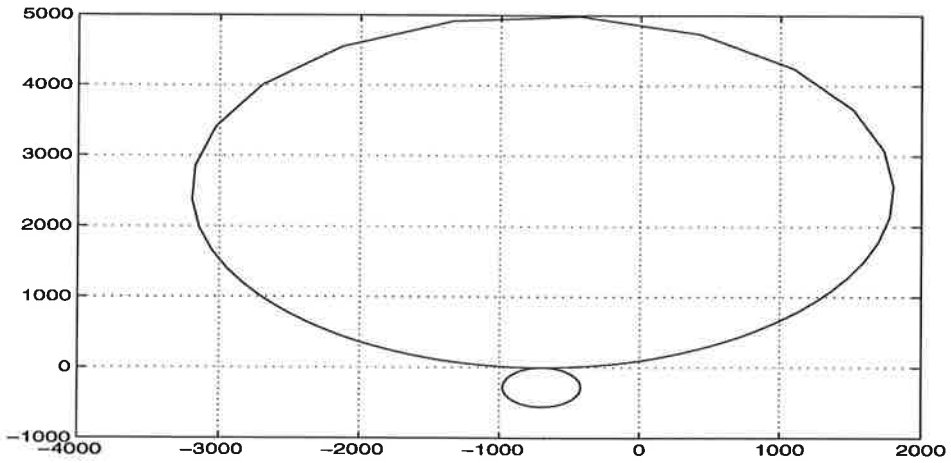

Figure 5.11: Example 2: Nyquist plot of the transformed forward system $\hat{G}(s)$

tiplier is probably better than the one used in the above mentioned paper. The following analysis is based on the use of this basis multiplier.

The multiplier which finally appears in the stability condition has the form

$$Z(j\omega) = d + x_1 H_1^*(j\omega)$$

where $H_1^*(j\omega) = -1/(s+10)$ is the complex conjugate of the Laplace transform of the basis multiplier $h_1(t)$ and d and x_1 are constants, the values of which are found using LMI-Lab. Its Bode plot is shown in Figure 5.12.

In Figures 5.13 and 5.14 the Nyquist and Bode plots of the product of $\hat{G}(j\omega)$ and the multiplier $Z(j\omega)$ have been plotted. The Nyquist plot lies completely in the open left half plane, which means that the stability condition is indeed satisfied. This can also be verified from the Bode plot, as the phase is always in the interval [-120,-180](degrees).

It should be mentioned here that this example is quite extreme, in the sense that the poles of $G(s)$ lie very close to the imaginary axis. However, it is useful from a computational point of view, as it makes clear that our algorithms can work efficiently even in so sensitive cases.

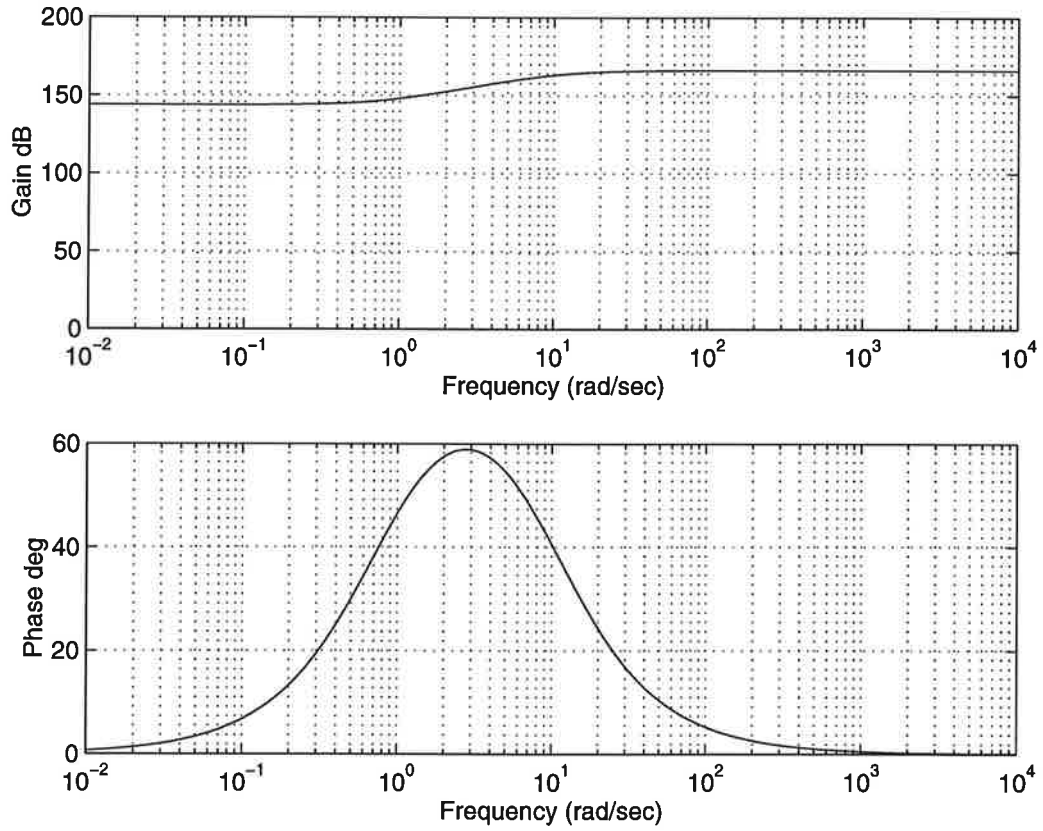

Figure 5.12: Example 2: Bode plot of $Z(j\omega) = d + x_1 H_1^*(j\omega).H_1(j\omega) = 1/(j\omega - 10)$ is the Fourier transform of the basis multiplier $h_1(t) = e^{10t}$

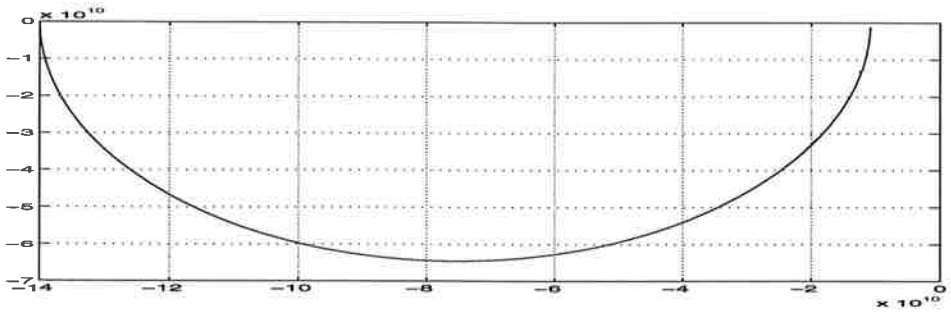

Figure 5.13: Example 2: Nyquist plot of the product of $\hat{G}(s)$ and $Z(j\omega)$

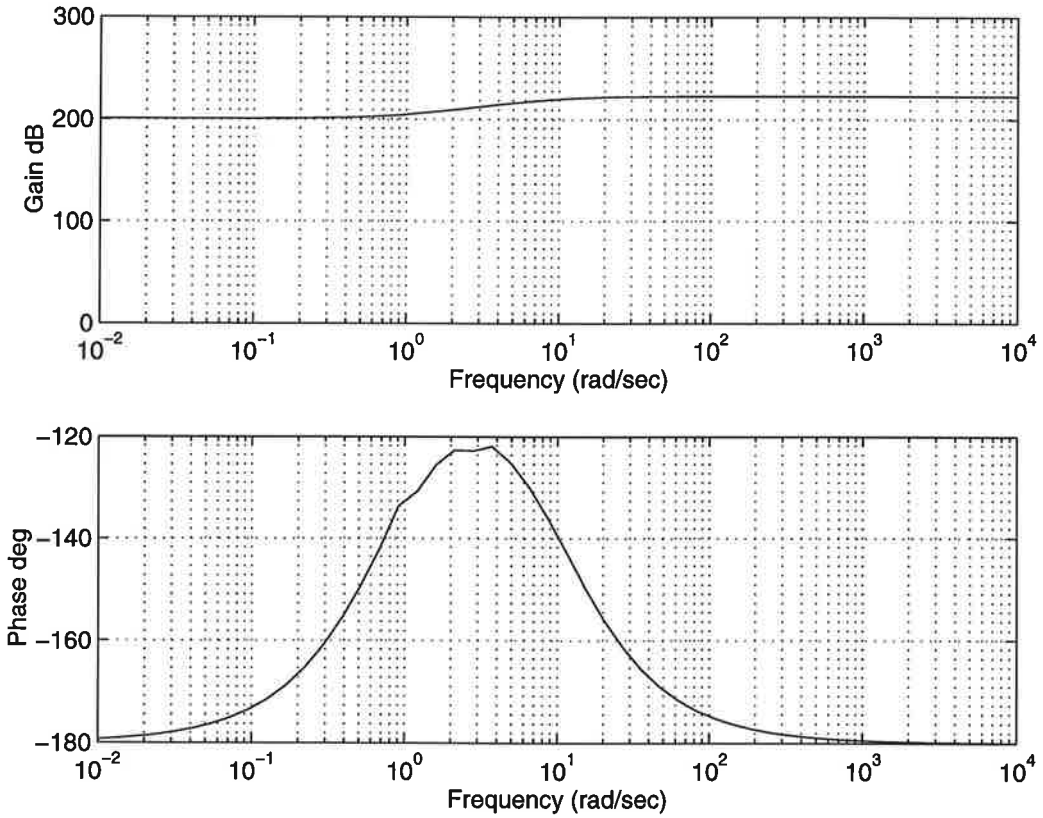

Figure 5.14: Example 2: Bode plot of the product of $\hat{G}(s)$ and $Z(j\omega)$

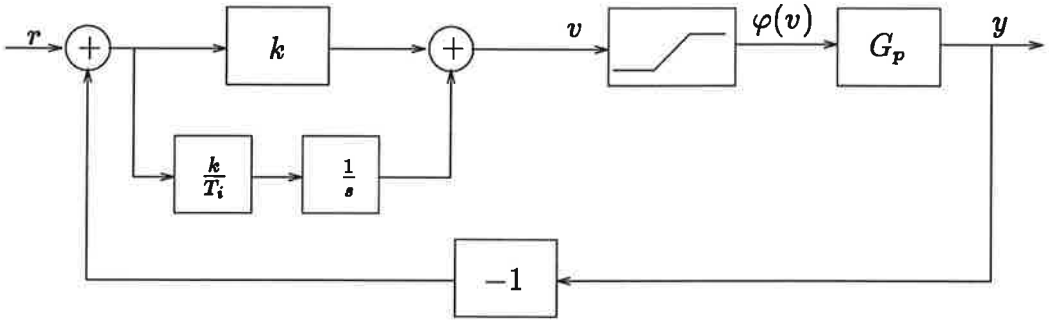

Figure 5.15: Control system with saturation and PID controller

5.3 Example 3

Consider the system shown in Figure 5.15. The system is controlled by a PI controller and the nonlinearity is a unit gain saturation.

The combination of a saturating actuator and a controller with integral action gives rise to a phenomenon called *integrator windup*. If the control error is so large that the integrator saturates, the feedback path will be broken because the actuator will remain saturated even if the process output changes. The integrator, being an unstable system, may then integrate up to a very large value. When the error changes sign, the integral may be so large that it takes considerable time until the integral assumes a normal value again.

There are several ways to avoid integrator windup. One possibility is to stop updating the integral when the actuator saturates. This method is called *conditional integration*.

Another method is the one called *tracking* and it is illustrated by the block diagram in Figure 5.16. In this system an extra feedback path is provided by measuring the actuator output and forming an error signal e_s as the difference between the actuator output and the controller output. This error is then fed back to the integrator through the gain $1/T_t$. The error signal e_s is zero when the actuator is not saturated. When the actuator is saturated, the extra feedback path tries to make the error signal e_s equal to zero. This means that the integrator is reset so that the controller output is at the saturation limit. The integrator is reset to an appropriate value with the time constant T_t, which is called the tracking-time constant. The advantage of this scheme for anti-windup is that it can be applied to any

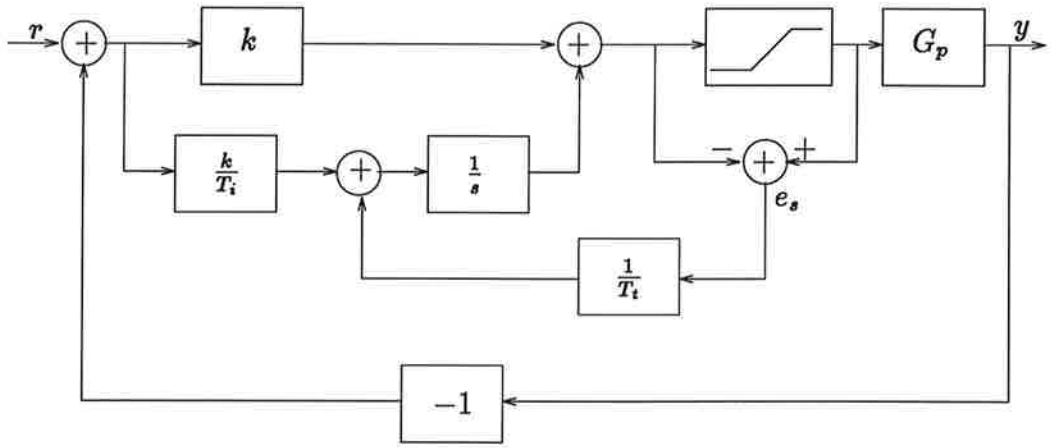

Figure 5.16: Regulator with anti-windup for the system of Figure 5.15

actuator, i.e. not only a saturated actuator, but also an actuator with arbitrary characteristics, such as a dead-zone or a hysteresis, as long as the actuator output can be measured. If this is not possible, the actuator can be modeled and an equivalent signal can be generated from the model.

The system of Figure 5.16 is equivalent to the one shown in Figure 5.17, which is of the general form shown in Figure 5.18.

We assume that the system dynamics are described by the transfer function

$$G_p(s) = \frac{1}{(s+1)^2(s+10)}$$

This can for example describe the system of a double tank controlled by a PI controller. The factor $1/(s+1)^2$ describes the tank dynamics, while the factor $1/(s+10)$ corresponds to a sensor measuring the liquid level in the lower tank. The saturation describes a pump [11].

The PI controller can be tuned using the Ziegler-Nichols method [4]. The parameters k and T_i are given by the following relationships:

$$k = 0.45k_0$$

$$T_i = \frac{T_0}{1.2}$$

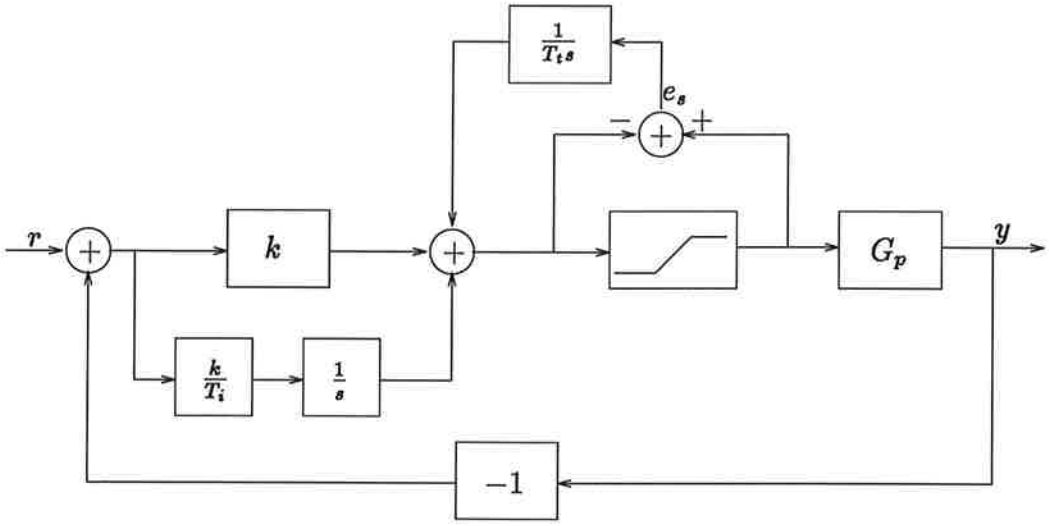

Figure 5.17: Regulator with anti-windup for the system of Figure 5.15

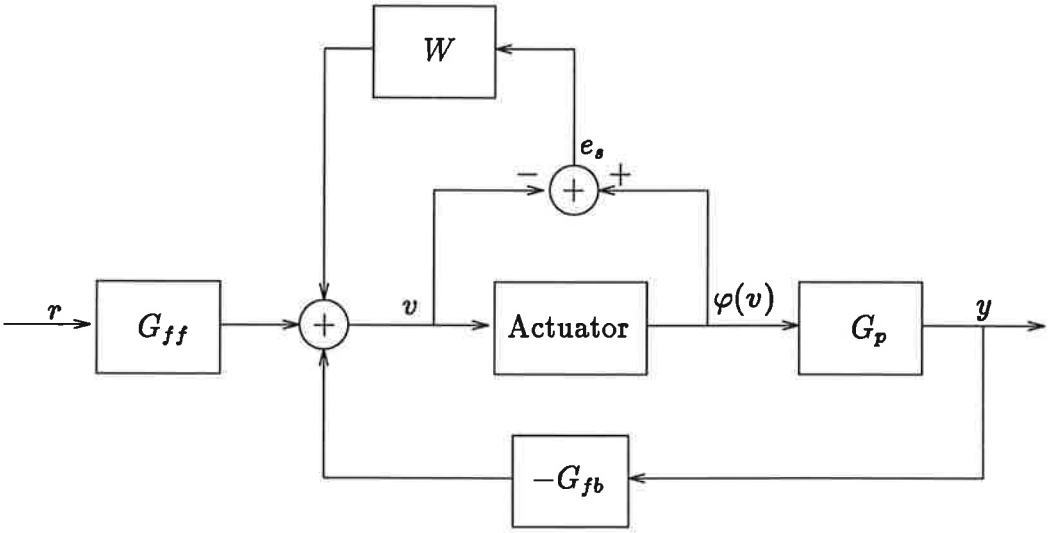

Figure 5.18: General form of control system with an actuator and anti-windup

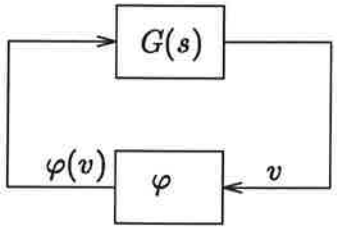

Figure 5.19: Closed loop system for stability analysis

where

$$k_0 = \frac{-1}{G_p(j\omega_0)}$$

$$T_0 = \frac{2\pi}{\omega_0}$$

and ω_0 is the frequency where the Nyquist plot of $G_p(j\omega)$ intersects the real axis. From the Nyquist plot of $G_p(s)$ it is easy to find that $\omega_0 = 4.58$ rad/sec. Hence

$$\begin{aligned} k_0 &= 242.37 \\ T_0 &= 1.37 \quad \text{sec} \\ k &= 109.07 \\ T_i &= 1.14 \quad \text{sec} \end{aligned}$$

The value of the tracking time constant T_t depends on the specific performance requirements. In any case though it has to be lower than the integrator constant T_i [11]. Since we are only concerned for the stability analysis of the system, the value $T_t = 1$ is sufficient for our purposes. Hence, the filter W of Figure 5.18 will be $W = 1/s$.

Our objective is to find the maximum value of the gain k for which the loop remains stable. In order to apply the method which has been presented in the previous chapters, the closed loop system of Figure 5.17 has to be brought in the form shown in Figure 5.19. We consider that the reference signal is zero, i.e. $r = 0$. From Figure 5.18 it is then easy to see that

$$\begin{aligned} v &= -G_{fb}y + W[\varphi(v) - v] \\ &= -G_{fb}G_p\varphi(v) + W\varphi(v) - Wv \end{aligned}$$

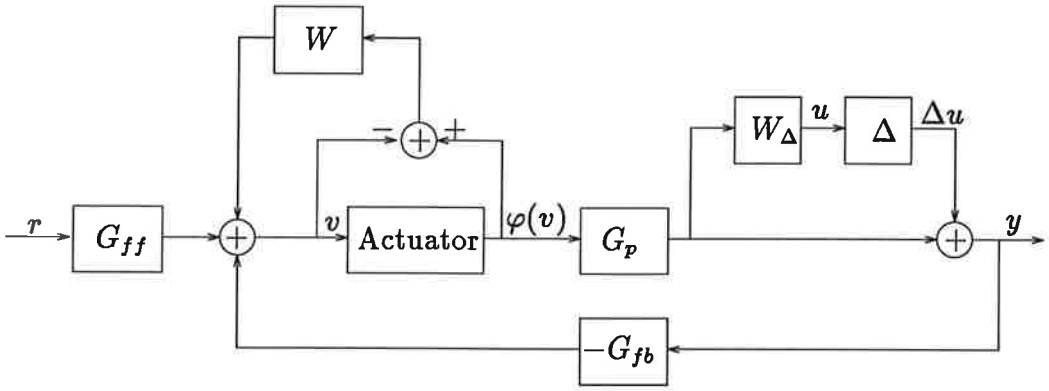

Figure 5.20: General form of control system with an actuator, multiplicative uncertainty and anti-windup

Hence

$$G = \frac{v}{\varphi(v)} = \frac{W - G_{fb}G_p}{1 + W}$$

The nonlinearity φ is a unit gain saturation. Hence, it can be considered as a slope restricted nonlinearity of the class slope$[0, 1]$.

LMI computations have been carried out using the above values for k, T_i and T_t. Several multipliers give stability of the closed loop system but the multiplier which allows the maximum value of the gain k has been found to be h(t) = exp(10t). The maximum gain is $k_{max} = 125.2$. Hence, we have a gain margin of 14.79 %.

We now consider the case of the existence of a multiplicative uncertainty in the system dynamics. G_p is considered to be the nominal value of the system transfer function. Its actual value is given as follows

$$G_{p,actual} = G_p(1 + W_\Delta \Delta).$$

Δ is assumed to be a linear time-invariant operator with gain $\|\Delta(j\omega)\| \leq 1$ and W_Δ is a high-pass filter. Hence, the uncertainty Δ affects the system only in high frequencies. The block diagram of the system is shown in Figure 5.20.

Our objective is again to find the multipliers which give the maximal upper bound of the gain k. Since we have two nonlinearities, in order to apply our method, we should transform the system of Figure 5.20 to the system

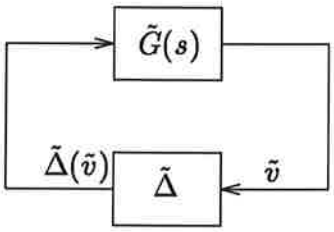

Figure 5.21: Closed loop system for stability analysis under the presence of a multiplicative uncertainty

shown in Figure 5.21.

In this system

$$\tilde{G} = \begin{bmatrix} G_{11} & G_{12} \\ G_{21} & G_{22} \end{bmatrix}, \quad \tilde{\Delta} = \begin{bmatrix} \varphi & 0 \\ 0 & \Delta \end{bmatrix}, \quad \tilde{v} = \begin{bmatrix} v \\ u \end{bmatrix} \quad \text{and} \quad \tilde{\Delta}(\tilde{v}) = \begin{bmatrix} \varphi(v) \\ \Delta(u) \end{bmatrix}$$

where

$$G_{11}(s) = \left.\frac{v(s)}{\varphi(v)(s)}\right|_{\Delta(u)=0} \qquad G_{12}(s) = \left.\frac{v(s)}{\Delta(u)(s)}\right|_{\varphi(v)=0}$$

$$G_{21}(s) = \left.\frac{u(s)}{\varphi(v)(s)}\right|_{\Delta(u)=0} \qquad G_{22}(s) = \left.\frac{u(s)}{\Delta(u)(s)}\right|_{\varphi(v)=0}$$

From Figure 5.20 it is easy to find that

$$G_{11}(s) = \frac{W - G_{fb}G_p}{1+W} \qquad G_{12}(s) = \frac{-G_{fb}}{1+W}$$

$$G_{21}(s) = W_\Delta G_p \qquad G_{22} = 0.$$

As it has been mentioned in previous chapters, a description of the operator $\tilde{\Delta} = \text{diag}\{\varphi, \Delta\}$ can be obtained simply by augmentation of the descriptions of the nonlinearity φ and the uncertainty Δ. φ is a unit gain saturation, hence it can be considered as a slope restricted nonlinearity of the class slope[0,1]. For the uncertainty Δ a corresponding IQC is defined by the matrix

$$\Pi_\Delta = \begin{bmatrix} R^*UR & 0 \\ 0 & -R^*UR \end{bmatrix}$$

where $U = U^T \geq 0$ [7]. In order to obtain the descriptions of φ and Δ, the functions Complexpar and ZamesFalb have been used respectively. The augmentation is obtained using the function IQCdaug. The corresponding Matlab program, Example3_b.m, is listed in Appendix B.

LMI computations have been carried out using the following data: $k = 109.07$, $T_i = 1.14$, $T_t = 1$. The filter W_Δ was chosen as

$$W_\Delta = \frac{s+10}{s+1000}$$

The multipliers which allow the highest gain k have been found to be:

For the saturation φ : $h(t) = exp(10t)$

For Δ : $R = \left[1 \quad \frac{s-0.1}{s+0.1} \quad \frac{(s-0.1)^2}{(s+0.1)^2}\right]^T$.

The maximum gain is $k_{max} = 120.7$. As it is expected, this gain is lower than the maximum gain which was achieved when the multiplicative uncertainty was not present.

5.4 Conclusions

The results that have been presented in the previous chapters have in this chapter been applied to three examples. The first two examples are just theoretical. They show how the theory can be applied to each specific case. Useful conclusions about the range of frequencies where the stability condition is not satisfied, as well as the kind of the multiplier that should be used, can be drawn from the Nyquist and Bode plots of the transformed forward system. In the third example a model of a physical system has been studied. Both the cases of a saturation and the simultaneous presence of a saturation and a multiplicative uncertainty have been considered. The usefulness of the IQC description of perturbations becomes evident here, as it is shown how easily the results can be extended to cases where more than one perurbation is present in the closed loop system. All LMI computations in this chapter have been performed by LMI Lab [9].

Conclusions

The object of this thesis was the stability analysis of control systems which include static nonlinearities and uncertainties. The analysis has been based on the concept of Integral Quadratic Constraints (IQC's).

A review of recent results in this area has first been made. The already known IQC's describing sector nonlinearities and slope restricted nonlinearities have been presented and discussed. A new IQC describing a friction model has been proved. The proposed friction model covers a lot of different types of friction appearing in control systems. This has been discussed in detail in chapter 3. A number of other nonlinearities commonly encountered in control systems has also been presented. It has been shown how these nonlinearities can be handled in the IQC framework.

A main point of the thesis has been the LMI formulation of the IQC results. Based on the results presented in [7], an LMI formulation of the IQC describing slope restricted nonlinearities has been derived. The proposed algorithm has also been programmed in Matlab. Particular emphasis has been given on the choice of multipliers for the case of slope restricted nonlinearities. We have suggested a way of choosing appropriate multipliers, based on useful conclusions that can be drawn from the Nyquist and Bode plots of the system transfer function.

Our results have been applied to three different systems. The two first are theoretical and they have also been studied in [13] and [5]. They are useful for presenting how the proposed method works and for illustrating the efficiency of the software. Furthermore, in one of them we have achieved results better than the ones in [5], which is a good indication for the proposed method of choosing multipliers.

The most important example though is the third one, where the stability of a model of a practical system controlled by a PI regulator with anti-windup

has been studied. The case of a unit gain saturation has been treated first. The next step was to consider a more general case by introducing a multiplicative uncertainty in the system's dynamics for high frequencies. It is shown that, once we have an IQC description for each nonlinearity or uncertainty, the analysis can be very easily extended to the case of many nonlinear or uncertain blocks. This is probably the most important feature of the IQC based analysis of nonlinear systems and a good motivation for using this method.

For the LMI computations in the examples the LMI-Toolbox of Matlab has been used. In some cases, especially when more than two multipliers are used, the computations become very complicated and time consuming. An improvement of the software with respect to the choice of multipliers would be a subject for further discussion. Finally, extension of the theory to cases of unbounded nonlinearities and hysteresis problems are subjects of great interest and open research areas.

Appendix A

Proofs

We are giving here the proofs of the theorems and the corollaries stated in Chapter 3.

A.1 Slope Restricted Nonlinearities

The following Lemmas [16] are useful for the proof of Theorem 3.1.

Lemma A.1 *If φ is monotone nondecreasing, then*

$$x\varphi(x) - y\varphi(x) \geq P(x) - P(y) \tag{A.1}$$

for all x and y, where $P(x) = \int_0^x \varphi(s)ds$.

Proof Since $\varphi(\cdot)$ is monotone nondecreasing, the following inequality will hold

$$[\varphi(x + k\Delta x) - \varphi(x)]k\Delta x \geq 0$$

for any integer $k \geq 0$. Hence

$$\sum_{k=1}^{m}[\varphi(x + k\Delta x) - \varphi(x)]\Delta x \geq 0$$

for any integer m. Setting $\Delta x = (y - x)/m$ and letting m approach infinity, we deduce that

$$\int_x^y \varphi(s)ds - \varphi(x)\int_x^y ds \geq 0. \tag{A.2}$$

Since $\int_x^y \varphi(s)ds = P(y) - P(x)$, (A.2) is equivalent to (A.1).

Lemma A.2 *If φ is monotone nondecreasing and if there is a constant $C > 0$ such that $|\varphi(x)| \leq C|x|$, then*

$$\int_{-\infty}^{\infty} x(t+\tau)\varphi(x(t))dt \leq \int_{-\infty}^{\infty} x(t)\varphi(x(t))dt \tag{A.3}$$

for all τ and any $x(\cdot)$ in $\boldsymbol{L}_2(-\infty,\infty)$. If, in addition, $\varphi(\cdot)$ is odd, then

$$\left|\int_{-\infty}^{\infty} x(t+\tau)\varphi(x(t))dt\right| \leq \int_{-\infty}^{\infty} x(t)\varphi(x(t))dt \tag{A.4}$$

for all τ and any $x(\cdot)$ in $\boldsymbol{L}_2(-\infty,\infty)$.

Proof Since $|\varphi(x)| \leq C|x|$ and $x(\cdot)$ is in $\mathbf{L}_2(-\infty,\infty)$, $\varphi(x(\cdot))$ is also in $\mathbf{L}_2(-\infty,\infty)$ and $P(x(\cdot))$ is in $\mathbf{L}_1(-\infty,\infty)$. Thus,

$$\begin{aligned}
&\int_{-\infty}^{\infty} \{x(t)\varphi(x(t)) - x(t+\tau)\varphi(x(t))\}dt \\
&\quad \geq \int_{-\infty}^{\infty} P(x(t))dt - \int_{-\infty}^{\infty} P(x(t+\tau))dt \\
&\quad = 0.
\end{aligned}$$

Hence (A.3) holds.
If φ is odd, then $P(\cdot)$ is even, and so

$$\begin{aligned}
&\int_{-\infty}^{\infty} \{x(t)\varphi(x(t)) + x(t+\tau)\varphi(x(t))\}dt \\
&\quad = \int_{-\infty}^{\infty} \{x(t)\varphi(x(t)) - [-x(t+\tau)]\varphi(x(t))\}dt \\
&\quad \geq \int_{-\infty}^{\infty} \{P(x(t)) - P(-x(t+\tau))\}dt \\
&\quad = 0.
\end{aligned}$$

Hence, (A.4) holds.

Proof of Theorem 3.1 We have to show that

$$\int_{-\infty}^{\infty} \begin{bmatrix} \hat{v}(j\omega) \\ \widehat{\varphi(v)}(j\omega) \end{bmatrix}^* \begin{bmatrix} 0 & d+H(j\omega) \\ d+H^*(j\omega) & 0 \end{bmatrix} \begin{bmatrix} \hat{v}(j\omega) \\ \widehat{\varphi(v)}(j\omega) \end{bmatrix} d\omega \geq 0 \tag{A.5}$$

for all $v \in \mathbf{L}_2[0,\infty)$.

The left side of equation (A.5) can be written as follows

$$L = \int_{-\infty}^{\infty} \Big\{ \hat{v}^*(j\omega)[d + H(j\omega)]\widehat{\varphi(v)}(j\omega) + \widehat{\varphi(v)}^*(j\omega)[d + H^*(j\omega)]\hat{v}(j\omega) \Big\} d\omega \qquad \text{(A.6)}$$

Using the property

$$\int_{-\infty}^{\infty} \hat{u}^*(j\omega)\hat{H}(j\omega)\hat{v}(j\omega)d\omega = \int_{-\infty}^{\infty} \hat{v}^*(j\omega)\hat{H}^*(j\omega)\hat{u}(j\omega)d\omega$$

equation (A.6) takes the form

$$\begin{aligned} L &= 2d\int_{-\infty}^{\infty} \hat{v}^*(j\omega)\widehat{\varphi(v)}(j\omega)d\omega + 2\int_{-\infty}^{\infty} \hat{v}^*(j\omega)H(j\omega)\widehat{\varphi(v)}(j\omega)d\omega \\ &= 2d\int_{-\infty}^{\infty} \hat{v}^*(j\omega)\widehat{\varphi(v)}(j\omega)d\omega + 2\int_{-\infty}^{\infty} \hat{v}^*(j\omega)\hat{z}(j\omega)d\omega \qquad \text{(A.7)} \end{aligned}$$

where $\hat{z}(j\omega) = H(j\omega)\widehat{\varphi(v)}(j\omega)$ is the Fourier transform of the signal

$$z(t) = h(t) * \varphi(v)(t) = \int_{-\infty}^{\infty} h(\tau)\varphi(v)(t-\tau)d\tau \qquad \text{(A.8)}$$

Applying Parseval's Theorem to (A.7) and using (A.8) we get

$$\begin{aligned} L &= 2d\frac{1}{2\pi}\int_{-\infty}^{\infty} v(t)\varphi(v)(t)dt + 2\frac{1}{2\pi}\int_{-\infty}^{\infty} v(t)z(t)dt \\ &= \frac{d}{\pi}\int_{-\infty}^{\infty} v(t)\varphi(v)(t)dt + \frac{1}{\pi}\int_{-\infty}^{\infty} v(t)\int_{-\infty}^{\infty} h(\tau)\varphi(v)(t-\tau)d\tau dt \qquad \text{(A.9)} \end{aligned}$$

By changing the order of integration in (A.9) we have

$$L = \frac{d}{\pi}\int_{-\infty}^{\infty} v(t)\varphi(v)(t)dt + \frac{1}{\pi}\int_{-\infty}^{\infty} h(\tau)\int_{-\infty}^{\infty} v(t)\varphi(v)(t-\tau)dtd\tau \qquad \text{(A.10)}$$

According to Lemma A.2 the following inequality holds

$$\begin{aligned} \left|\int_{-\infty}^{\infty} v(t)\varphi(v)(t-\tau)dt\right| &\leq \int_{-\infty}^{\infty} v(t-\tau)\varphi(v)(t-\tau)dt \\ &= \int_{-\infty}^{\infty} v(t)\varphi(v)(t)dt \qquad \text{(A.11)} \end{aligned}$$

The integral $J = \int_{-\infty}^{\infty} v(t)\varphi(v)(t)dt$ is always nonnegative, since φ is odd and nondecreasing. Hence

$$h(\tau)\int_{-\infty}^{\infty} v(t)\varphi(v)(t-\tau)dt \;\geq\; -\left|h(\tau)\int_{-\infty}^{\infty} v(t)\varphi(v)(t-\tau)dt\right| =$$

$$-|h(\tau)|\left|\int_{-\infty}^{\infty} v(t)\varphi(v)(t-\tau)dt\right| \;\geq\; -|h(\tau)|\int_{-\infty}^{\infty} v(t)\varphi(v)(t)dt$$

By integrating both sides of the above inequality we get

$$\begin{aligned}&\int_{-\infty}^{\infty} h(\tau)\int_{-\infty}^{\infty} v(t)\varphi(v)(t-\tau)dtd\tau \\ &\geq -\int_{-\infty}^{\infty} |h(\tau)|\int_{-\infty}^{\infty} v(t)\varphi(v)(t)dtd\tau \end{aligned} \tag{A.12}$$

Using inequality (A.12), equation (A.10) yields

$$\begin{aligned} L \;&\geq\; \frac{d}{\pi}\int_{-\infty}^{\infty} v(t)\varphi(v)(t)dt - \frac{1}{\pi}\int_{-\infty}^{\infty} |h(\tau)|\int_{-\infty}^{\infty} v(t)\varphi(v)(t)dtd\tau \\ &=\; \frac{1}{\pi}\left[d - \int_{-\infty}^{\infty} |h(\tau)|d\tau\right]J \end{aligned} \tag{A.13}$$

Since $J \geq 0$ and the L_1-norm of $h(t)$ is no larger than d, the right part of the inequality A.13 is always nonnegative. Hence, φ satisfies the IQC defined by

$$\Pi(j\omega) = \begin{bmatrix} 0 & d + H(j\omega) \\ d + H^*(j\omega) & 0 \end{bmatrix}$$

Remark When φ is not odd, the theorem can be proven in a similar way. The only change is that we need to make use of (A.3) instead of (A.4) in Lemma A.2.

Proof of Corollary 3.1 Transform the vector $[\hat{v}(j\omega) \quad \widehat{\varphi(v)}(j\omega)]^T$ as follows

1st Transformation :

$$\begin{bmatrix} \hat{v}(j\omega) \\ \tilde{\varphi}(v)(j\omega) \end{bmatrix} = \begin{bmatrix} 1 & 0 \\ -\alpha & 1 \end{bmatrix}\begin{bmatrix} \hat{v}(j\omega) \\ \widehat{\varphi(v)}(j\omega) \end{bmatrix}$$

2nd Transformation :

$$\begin{bmatrix} \hat{y}(j\omega) \\ \widehat{N(y)}(j\omega) \end{bmatrix} = \begin{bmatrix} 1 & \frac{-1}{\beta-\alpha} \\ 0 & 1 \end{bmatrix}\begin{bmatrix} \hat{v}(j\omega) \\ \tilde{\varphi}(v)(j\omega) \end{bmatrix}$$

The operator $\tilde{\varphi}(\cdot)$ is defined as

$$\tilde{\varphi}(x) = \varphi(x) - \alpha x \tag{A.14}$$

It has the same properties as φ and it satisfies the condition

$$0 \leq \frac{\tilde{\varphi}(x_1) - \tilde{\varphi}(x_2)}{x_1 - x_2} \leq \beta - \alpha - \varepsilon \tag{A.15}$$

From the second transformation it follows that

$$y(\cdot) = v(\cdot) - \frac{1}{\beta - \alpha}\tilde{\varphi}(v)(\cdot) \tag{A.16}$$

$$N(y)(\cdot) = \tilde{\varphi}(v)(\cdot) \tag{A.17}$$

It is now sufficient to show that N has all the properties that φ has. Then the corollary follows from Theorem 2. More specifically, we will show that
(i) $N(0) = 0$,
(ii) N is monotone nondecreasing,i.e. $(y_1 - y_2)[N(y_1) - N(y_2)] \geq 0$,

(iii) $0 \leq \frac{N(y_1)-N(y_2)}{y_1-y_2} \leq M < \infty, \quad \forall \quad y_1 \neq y_2$,
(iv) N is odd.

The proofs of the above properties are given below.

Property (i)
For $y = 0$, equation A.16 gives

$$v = \frac{1}{\beta - \alpha}\tilde{\varphi}(v) \tag{A.18}$$

Equation (A.15) for $x_1 = x$ and $x_2 = 0$ yields

$$0 \leq \frac{\tilde{\varphi}(x)}{x} \leq \beta - \alpha - \varepsilon < \beta - \alpha$$

Hence, for $x > 0$ it holds that $0 \leq \tilde{\varphi}(x) < (\beta - \alpha)x$ and for $x < 0$ it holds that $0 \geq \tilde{\varphi}(x) > (\beta - \alpha)x$. The above inequalities can be written together as

$$0 \leq \left|\tilde{\varphi}(x)\right| < (\beta - \alpha)|x|, \quad \forall x \neq 0 \tag{A.19}$$

Because of inequality A.19, equation A.18 holds if and only if $v = \tilde{\varphi}(v) = 0$. Hence, A.17 yields $N(0) = 0$.

Property (ii)
According to equations (A.16) and (A.17) the following equalities hold

$$\begin{aligned}
(y_1 - y_2)\big[N(y_1) - N(y_2)\big] &= \left[v_1 - \frac{1}{\beta-\alpha}\tilde{\varphi}(v_1) - v_2 + \frac{1}{\beta-\alpha}\tilde{\varphi}(v_2)\right]\big[\tilde{\varphi}(v_1) - \tilde{\varphi}(v_2)\big] \\
&= \left[(v_1 - v_2) - \frac{1}{\beta-\alpha}\big[\tilde{\varphi}(v_1) - \tilde{\varphi}(v_2)\big]\right]\big[\tilde{\varphi}(v_1) - \tilde{\varphi}(v_2)\big] \\
&= (v_1 - v_2)\big[\tilde{\varphi}(v_1) - \tilde{\varphi}(v_2)\big]\left[1 - \frac{1}{\beta-\alpha}\frac{\big[\tilde{\varphi}(v_1) - \tilde{\varphi}(v_2)\big]}{v_1 - v_2}\right]
\end{aligned}$$

Since $\tilde{\varphi}$ is nondecreasing, it holds that $(v_1 - v_2)\big[\tilde{\varphi}(v_1) - \tilde{\varphi}(v_2)\big] \geq 0$. From (A.15) it is easy to see that

$$1 - \frac{1}{\beta-\alpha}\frac{\big[\tilde{\varphi}(v_1) - \tilde{\varphi}(v_2)\big]}{v_1 - v_2} \geq 0$$

Hence, $(y_1 - y_2)\big[N(y_1) - N(y_2)\big] \geq 0$.

Property (iii)

$$\begin{aligned}
\frac{N(y_1) - N(y_2)}{y_1 - y_2} &= \frac{\tilde{\varphi}(v_1) - \tilde{\varphi}(v_2)}{v_1 - \frac{1}{\beta-\alpha}\tilde{\varphi}(v_1) - v_2 + \frac{1}{\beta-\alpha}\tilde{\varphi}(v_2)} \\
&= \frac{\tilde{\varphi}(v_1) - \tilde{\varphi}(v_2)}{(v_1 - v_2) - \frac{1}{\beta-\alpha}\big[\tilde{\varphi}(v_1) - \tilde{\varphi}(v_2)\big]} \\
&= \frac{\frac{\tilde{\varphi}(v_1) - \tilde{\varphi}(v_2)}{v_1 - v_2}}{1 - \frac{1}{\beta-\alpha}\frac{\big[\tilde{\varphi}(v_1) - \tilde{\varphi}(v_2)\big]}{v_1 - v_2}} \qquad \text{(A.20)}
\end{aligned}$$

Using (A.15), equation (A.20) yields

$$0 \leq \frac{N(y_1) - N(y_2)}{y_1 - y_2} \leq \frac{(\beta-\alpha)(\beta-\alpha-\varepsilon)}{\varepsilon} = M < \infty.$$

Property (iv)
Equation (A.16) yields

$$-y = -v + \frac{1}{\beta-\alpha}\tilde{\varphi}(v) \qquad \text{(A.21)}$$

Since φ is odd, (A.21) can be written as follows

$$-y = -v - \frac{1}{\beta - \alpha}\tilde{\varphi}(-v) \tag{A.22}$$

Taking into account (A.22), equation (A.17) yields

$$N(-y) = \tilde{\varphi}(-v) = -\tilde{\varphi}(v) = -N(y)$$

Hence, N is odd.

Since N has all the properties mentioned in Theorem 2, N will satisfy the IQC defined by

$$\Pi(j\omega) = \begin{bmatrix} 0 & d + H(j\omega) \\ d + H^*(j\omega) & 0 \end{bmatrix}$$

and the corollary follows.

A.2 A Friction Model

Proof of Theorem 3.3 Consider the following quantity

$$\begin{aligned}
A &= \Big[[u(t) - k_2 v(t)] + [h * (u - k_2 v)](t)\Big]\Big[v(t) - \frac{1}{k_1}u(t)\Big] \\
&= [u(t) - k_2 v(t)]\Big[v(t) - \frac{1}{k_1}u(t)\Big] \\
&\qquad + \int_{-\infty}^{\infty} h(\tau)(u - k_2 v)(t - \tau)d\tau \Big[v(t) - \frac{1}{k_1}u(t)\Big] \\
&\geq [u(t) - k_2 v(t)]\Big[v(t) - \frac{1}{k_1}u(t)\Big] \\
&\qquad - \Big|\int_{-\infty}^{\infty} h(\tau)(u - k_2 v)(t - \tau)d\tau\Big|\Big|v(t) - \frac{1}{k_1}u(t)\Big| \\
&\geq [u(t) - k_2 v(t)]\Big[v(t) - \frac{1}{k_1}u(t)\Big] \\
&\qquad - \int_{-\infty}^{\infty} |h(\tau)|d\tau \quad \sup_t \big\{\big|(u - k_2 v)(t)\big|\big\}\Big|v(t) - \frac{1}{k_1}u(t)\Big| \\
&\geq [u(t) - k_2 v(t)]\Big[v(t) - \frac{1}{k_1}u(t)\Big] - C\Big|v(t) - \frac{1}{k_1}u(t)\Big|
\end{aligned} \tag{A.23}$$

where we have made the assumption that the L_1-norm of the impulse response of H is no larger than a positive constant α, i.e.

$$\int_{-\infty}^{\infty} |h(t)|dt \leq \alpha$$

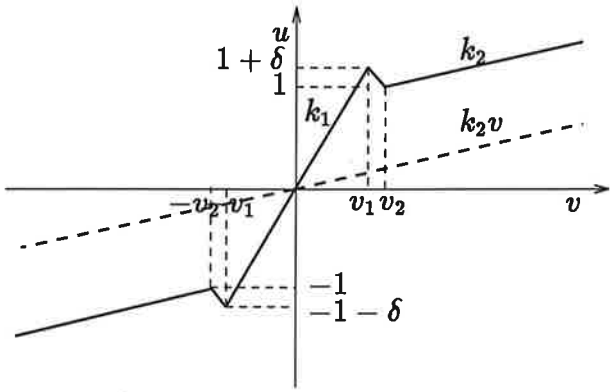

Figure A.1:

and

$$C = \alpha \sup_t \{|(u - k_2 v)(t)|\} \tag{A.24}$$

From Figure A.1 it is easy to see that

$$\forall t, \quad |(u - k_2 v)(t)| \leq (1 + \delta) - k_2 v_1 = \sup_t \{|(u - k_2 v)(t)|\} \tag{A.25}$$

From Figure 3.3 we can see that:
(i) For $|v(t)| \leq |v_1|$, $u(t) = k_1 v(t)$ and hence A=0.
(ii) For $v(t) > v_1$, $k_1 v(t) > u(t)$. Hence (A.23) yields

$$A \geq [u(t) - k_2 v(t) - C]\left[v(t) - \frac{1}{k_1} u(t)\right] \tag{A.26}$$

Assuming that

$$\begin{aligned} C &= \inf_{v > v_1} [u(t) - k_2 v(t)] \\ \text{i.e.} \quad C &= u(v_2) - k_2 v_2 = 1 - k_2 v_2 \end{aligned} \tag{A.27}$$

(A.26) yields $A \geq 0$, $\forall v(t) > v_1$.
(iii) For $v(t) < -v_1$, $k_1 v(t) < u(t)$. Hence,

$$A \geq [u(t) - k_2 v(t) + C]\left[v(t) - \frac{1}{k_1} u(t)\right]$$

In this case,

$$C = \inf_{v > v_1} [u(t) - k_2 v(t)] = - \sup_{v < -v_1} [u(t) - k_2 v(t)]$$

and $A \geq 0, \quad \forall v(t) < -v_1$.

From equations (A.24), (A.25) and (A.27) we find that the bound of the L_1-norm of the impulse response of H should be

$$\alpha = \frac{1 - k_2 v_2}{(1+\delta) - k_2 v_1}$$

Since

$$\left[v(t) - \frac{1}{k_1}u(t)\right]\left[[u(t) - k_2 v(t)] + [h * (u - k_2 v)](t)\right] \geq 0, \quad \forall t$$

the following inequality will also hold

$$\int_{-\infty}^{\infty} \left[v(t) - \frac{1}{k_1}u(t)\right]\left[[u(t) - k_2 v(t)] + [h * (u - k_2 v)](t)\right] dt \geq 0 \quad \text{(A.28)}$$

Applying Parseval's theorem to (A.28) we get

$$\begin{aligned}
& 2\pi \int_{-\infty}^{\infty} \left(\hat{v} - \frac{1}{k_1}\hat{u}\right)^*(j\omega)[\hat{u} - k_2\hat{v} + H(\hat{u} - k_2\hat{v})](j\omega)d\omega \geq 0 \\
\Leftrightarrow \quad & 2\int_{-\infty}^{\infty} \left(\hat{v}^* - \frac{1}{k_1}\hat{u}^*\right)(j\omega)\left[1 + H(j\omega)\right](\hat{u} - k_2\hat{v})(j\omega)d\omega \geq 0 \\
\Leftrightarrow \quad & \int_{-\infty}^{\infty} \left(\hat{v}^* - \frac{1}{k_1}\hat{u}^*\right)(j\omega)\left[1 + H(j\omega)\right](\hat{u} - k_2\hat{v})(j\omega)d\omega \\
+ \quad & \int_{-\infty}^{\infty} (\hat{u}^* - k_2\hat{v}^*)(j\omega)\left[1 + H^*(j\omega)\right]\left(\hat{v} - \frac{1}{k_1}\hat{u}\right)(j\omega)d\omega \geq 0 \\
\Leftrightarrow \quad & \int_{-\infty}^{\infty} \begin{bmatrix} \left(\hat{v} - \frac{1}{k_1}\hat{u}\right)(j\omega) \\ (\hat{u} - k_2\hat{v})(j\omega) \end{bmatrix}^* \Pi(j\omega) \begin{bmatrix} \left(\hat{v} - \frac{1}{k_1}\hat{u}\right)(j\omega) \\ (\hat{u} - k_2\hat{v})(j\omega) \end{bmatrix} d\omega \geq 0 \\
\Leftrightarrow \quad & \int_{-\infty}^{\infty} \begin{bmatrix} \hat{v} \\ \hat{u} \end{bmatrix}^* \begin{bmatrix} 1 & -\frac{1}{k_1} \\ -k_2 & 1 \end{bmatrix}^T \Pi(j\omega) \begin{bmatrix} 1 & -\frac{1}{k_1} \\ -k_2 & 1 \end{bmatrix} \begin{bmatrix} \hat{v} \\ \hat{u} \end{bmatrix}
\end{aligned}$$

where

$$\Pi(j\omega) = \begin{bmatrix} 0 & 1 + H(j\omega) \\ 1 + H^*(j\omega) & 0 \end{bmatrix}.$$

Hence φ satisfies the IQC defined by

$$\bar{\Pi}(j\omega) = \begin{bmatrix} 1 & -\frac{1}{k_1} \\ -k_2 & 1 \end{bmatrix}^T \Pi(j\omega) \begin{bmatrix} 1 & -\frac{1}{k_1} \\ -k_2 & 1 \end{bmatrix}.$$

Appendix B

Matlab Programs

The programs and functions presented in this appendix are all written in the Matlab-4.2c programming code.

The function **slopeNL.m** provides the LMI formulation of the IQC describing slope restricted nonlinearities.

The program **Example1.m** has been used for the computations concerning the first example. For the second example exactly the same code has been used, so it is not going to be given again.

The programs **Example3_a.m** and **Example3_b.m** refer to the third example. The first one considers the case when just a saturation is present and the second one the case of the simultaneous presence of a saturation and an uncertainty.

The function **mult_plot.m** has been used in order to obtain the Bode plot of the multiplier appearing in the stability condition. Its inputs are the multiplier and the results, Mstruc, of the IQCfeas command.

At some points there are references to functions which are not listed here. These were part of already existing software, written by Ulf Jönsson, Technical University of Lund, which has been used for the LMI computations. A list and a short description of these functions is given below.

IQCfeas : It examines the feasibility test as this has been presented in section 4.1. It has the following structure
[Mstruc,tmin] = IQCfeas(G,IQCdata,plot_type,wvec), where

G : System matrix obtained with the mu-tools command pck

IQCdata :	A set of IQC's
plot_type :	'none' (default) No plot.
	'FDI0' Plot largest eigenvalue corrsponding to the FDI (0) above.
	'all FDIs' Plot largest eigenvalue corrsponding to the FDIs in (0),...,(N) in separate windows.
wvec :	The FDI plots are calculated at these frequencies. By default wvec=logspace(-2,2).

Mstruc is the $M(\lambda)$ matrix, see section 4.2. If the feasibility test is succesful then tmin is negative, otherwise positive.

IQCdaug : This function generates the set of IQC's satisfied by the operator $\text{diag}(\Delta_1, \ldots, \Delta_N)$ from given sets of Integral Quadratic Constraints satisfied by operators $\Delta_1, \ldots, \Delta_N$, It is currently limited to nine input arguments. The way the augmentation is achieved is the one discussed in chapter 2.

Complexpar : This function specifies a set of IQC's corresponding to a bounded complex parameter $\Delta = \delta I$. The size of the identity matrix corresponds to the column size of the multiplier. δ can be a scalar LTI system, such that $\|\delta(j\omega)\| \leq 1$ or a constant parameter, such that $|\delta| \leq 1$. The function is defined as follows
IQCdata = Complexpar(R,bound),
where R is the multiplier. 'bound' is the bound on the multipliers, which by default is infinity. The corresponding Π matrix is as shown in section 5.3.

slopeNL.m

```
function IQCdata = slopeNL(mult,alpha,beta);
%
%  IQCdata = slopeNL(mult,alpha,beta);
%
%  Specifies a set of IQC's corresponding to a possible nonlinear and
%  time-varying bounded operator Delta which has the following properties:
%  (i)   Delta(0)=0
%  (ii)  Delta is monotone nondecreasing
%  (iii) There is k>0 such that |Delta(x)| <= k|x|, for any x
%  (iv)  Delta is odd
%
%  Pi(jw) is given as
%
%          [   0         d + H(jw)]
%  Pi(jw)= [                      ]
%          [d + H*(jw)       0    ]
%
%  where d is a nonnegative constant and H is a strictly proper function
%  in RLinf with the L1-norm of its impulse response no larger than d.
%
%  In the case of a single multiplier H, the following matrices are used.
%
%          [0   1]           [-1 ]          [ 1  0  0 ]
%          [0   H]           [|H|]          [ 0  1  0 ]
%   Phi0 = [0  -H]    Phi1 = [|H|]     Phi2=[ 0  0  1 ]
%          [1   0]           [ 1 ]          [-1  0  0 ]
%          [1   0]           [ 1 ]          [ 0 -1  0 ]
%          [1   0]           [ 1 ]          [ 0  0 -1 ]
%%
%         [0  0  0  d  0  0 ]
%         [0  0  0  0  x+ 0 ]
%  Mstruc=[0  0  0  0  0  x-]   M0=zeros(6)
%         [d  0  0  0  0  0 ]
%         [0  x+ 0  0  0  0 ]
%         [0  0  x- 0  0  0 ]
%
%  In the case of a nonlinearity Delta having all the properties mentioned
%  above and also
%
%             Delta(x1) - Delta(x2)
%   alpha <= ---------------------- <= beta - e,  beta-e > alpha,   e>0
%                   x1 - x2
%
%  the definitions of all the matrices above, apart from Phi0, remain
%  the same.
%
%  Phi0 is substituted by Phi0*T1*T2, where T1, T2 are the following
```

```
%  transformation matrices
%
%       [                -1       ]
%       [  1       ------------   ]             [ 1       0 ]
%  T1 = [           beta-alpha     ]       T2 = [             ]
%       [                         ]             [-alpha   1 ]
%       [  0             1        ]
%
%
%  If H is a linear combination of basis multipliers H1,H2,...,HN,
%  then the above matrices have to be transformed appropriately. Their
%  structure though will be similar to the one corresponding to N=1.
%
%  The inputs of the function are the multiplier vector, mult, and the
%  bounds of the nonlinearity, alpha and beta.
%
%  The multiplier vector has to be in the form
%
%    mult = [k1 l1 k2 l2 ... kN lN]
%
%  where each pair (ki,li) corresponds to a basis multiplier
%  (t^ki)*exp(li*t).
%
%
%

c = size(mult,2);       % Number of elements of multiplier vector
N = c/2;                % Number of basis multipliers
j=0;
for i = 1:2:c-1
    j = j+1;
    k(j) = mult(i);     % Power of t
    l(j) = mult(i+1);   % Coefficient in exponential
end

%  Find the Laplace transform of each basis multiplier.
%  This is based on the fact that the Laplace transform of
%  a function (t^ki)*exp(li*t) is h(s) = (ki!)/(s-li)^(ki+1)
%

H = [];                 % Initialization of vector H, which will
                        % be used for building the matrix Phi0
phi1 = -1;              % Initialization of the vector Phi1
for i=1:N
    k_fact = 1;
    den = [1 -l(i)];
    for j=1:k(i)
        k_fact = k_fact*j;          % k-factorial
        den = conv(den,[1 -l(i)]);  % Denominator of H(s)
```

```
    end;
    num = k_fact;                    % Numerator of H(s)

    [a,b,c,d] = tf2ss(num,den);
    h = pck(a,b,c,d);                % Basis multiplier h
    H=abv(H,h,mscl(h,-1));
    normh = abs(k_fact/((l(i))^(k(i)+1))); % Norm of h
    phi1 = abv(phi1,normh,normh);
end;


if nargin==1     % Case of a nonlinearity having the properties (i)-(iv)

   Phi0 = sbs(abv(zeros((2*N+1),1),ones((2*N+1),1)), ...
              abv(1,H,zeros((2*N+1),1)));

else             % Case of a nonlinearity having the properties (i)-(iv)
                 % and also slope in the interval [alpha, beta-e]

   T1 = [1 -1/(beta-alpha) ;  0  1];
   T2 = [1 0 ; -alpha 1];
   Phi0 = mmult(sbs(abv(zeros((2*N+1),1),ones((2*N+1),1)), ...
                    abv(1,H,zeros((2*N+1),1))),T1,T2);
end;

Fiset = putsys(Phi0,Fiset);
Phi1 = abv(phi1,ones((2*N+1),1))
Fiset = putsys(Phi1,Fiset);
Phi2 = [eye(2*N+1); -eye(2*N+1)];
Fiset = putsys(Phi2,Fiset);

D = 1;
for i=2:2*N+1
    D = daug(D,i)
end;

Mstruc = [zeros(2*N+1) D;
          D zeros(2*N+1)];

M0=0*Mstruc;
IQCdata = IQCpck(Mstruc,M0,Fiset);
```

Example1.m

```
%  Example 1

%  System transfer function G(s)
%  G(s)= 3(s+1)/(s^2)(s^2+s+25)

clear all;

% Define the system transfer function G(s)
num_G = 3*[1 1];
den_G = conv([1 0 0],[1 1 25]);
[A,B,C,D] = tf2ss(num_G,den_G);
G = pck(A,B,C,D);
frs_G=frsp(G,logspace(-2,2));

% Define the transfer function -G(s)
num_G_minus = -num_G;
den_G_minus = den_G;
G_minus = mscl(G,-1);
frs_G_minus = frsp(G_minus,logspace(-2,4));

% Specify the bounds of the slope of the nonlinearity
a = 1;
b = 7.9999;

% Choose the multiplier
multiplier = [1 1]
IQC=slopeNL(multiplier,a,b);
[Mstruc tmin]=IQCfeas(G_minus,IQC,'FDI0',logspace(-2,2))
grid;

% Bode and Nyquist plots of G(s)
figure(2); clg;
  bode(num_G,den_G,logspace(-2,2,10000));
  title('Bode Plot of the Transfer Function G(s)');
  subplot(3,1,3);
  vplot('nyq',frs_G);
  grid;
  title('Nyquist Plot of the Transfer Function G(s)');

% Nyquist plots of transformed forward system
figure(3); clg;
  % System G-tilde
  subplot(2,1,1);
  num_f1=a;
  den_f1=1;
  [num_cl1,den_cl1] = feedback(num_G_minus,den_G_minus,
                               num_f1,den_f1,1);
```

```
  [a_cl1,b_cl1,c_cl1,d_cl1] = tf2ss(num_cl1,den_cl1);
  G_tilde = pck(a_cl1,b_cl1,c_cl1,d_cl1);
  frs_cl1 = frsp(G_tilde,logspace(-1,2,1000));
  vplot('nyq', frs_cl1);
  grid;
  title('Nyquist Plot of Closed Loop with Transfer function -G(s)
        and Gain Feedback k=1');
  subplot(2,1,2);
    % System G_hat
    num_f2=-1;
    den_f2=b-a;
    [num_cl2,den_cl2]=parallel(num_cl1,den_cl1,num_f2,den_f2);
    [a_cl2,b_cl2,c_cl2,d_cl2] = tf2ss(num_cl2,den_cl2);
    G_hat = pck(a_cl2,b_cl2,c_cl2,d_cl2);
    frs_cl2 = frsp(G_hat,logspace(-1,2,1000));
    vplot('nyq',frs_cl2);
    grid;
    title('Nyquist Plot of the Transformed Forward System');

% Bode Plot of the Transformed Forward System
figure(4); clg;
  bode(num_cl2,den_cl2,logspace(-2,2));
  subplot(2,1,1);
  title('Bode Plot of the Transformed Forward System');


% Find and plot the multiplier which appears in the stability condition
H = mult_plot(Mstruc,multiplier);

% Check if the stability condition is satisfied
% Nyquist plot of the system appearing in the stability condition
figure(7); clg;
  sys = mmult(G_hat,H);
  frs = frsp(sys,logspace(-2,2,1000));
  vplot('nyq',frs);
  grid;
  title('Nyquist plot of the product of the transformed
        forward system and the multiplier');

% Bode plot of the system appearing in the stability condition
figure(8); clg;
  [a_syst_mult,b_syst_mult,c_syst_mult,d_syst_mult] = unpck(sys);
  [num_syst_mult,den_syst_mult] =
          ss2tf(a_syst_mult,b_syst_mult,c_syst_mult,d_syst_mult);
  bode(num_syst_mult,den_syst_mult,logspace(-2,2,1000));
  subplot(2,1,1);
  title('Bode plot of the product of the transformed forward
        system and the multiplier');
```

Example3a.m

```
% Example 3
% Saturation

clear all;

% System transfer function Gp(s)
num = 1;
den = conv(conv([1 1],[1 1]),[1 10]);

% PI Controller
k     = 125.2;  %116.1; %109.07;
Ti    = 1.1426;
num_c = k*[Ti 1];
den_c = [Ti 0];

% Filter W(s) for Anti-Windup
T = 1;
num_f = 1;
den_f = [T 0];

% System G(s) used in the IQC
num_G = addpoly(Ti*conv([1 2 1],[1 10]), -T*k*[Ti 1]);
den_G = Ti*conv(conv([T 1],[1 10]),[1 2 1]);
[A,B,C,D] = tf2ss(num_G,den_G);
G = pck(A,B,C,D);
w = logspace(-2,2,1000);
frs_G = frsp(G,w);

% Slope bounds for the saturation
a = 0;
b = 1;

% Choose the multiplier
multiplier = [0 10];
IQC=slopeNL(multiplier,0,1);
[Mstruc tmin]=IQCfeas(G,IQC,'FDI0',logspace(-2,2))
grid;

% Nyquist plot of transformed forward system
figure(4); clg;
  G_hat = madd(G, -1/b);
  frs_cl = frsp(G_hat,w);
  vplot('nyq',frs_cl);
  grid;
  title('Nyquist Plot of the Transformed Forward System');
```

```
% Bode Plot of the Transformed Forward System
figure(5); clg;
  [a_cl,b_cl,c_cl,d_cl] = unpck(G_hat);
  [num_cl,den_cl] = ss2tf(a_cl,b_cl,c_cl,d_cl);
  bode(num_cl,den_cl,logspace(-2,4));
  subplot(2,1,1);
  title('Bode Plot of the Transformed Forward System');

% Find and plot the multiplier which appears in the stability condition
H = mult_plot(Mstruc,multiplier);

% Check if the stability condition is satisfied
% Nyquist plot of the system appearing in the stability condition
figure(9); clg;
  sys = mmult(G_hat,H);
  frs = frsp(sys,logspace(-2,4,1000));
  vplot('nyq',frs);
  grid;
  title('Nyquist plot of the product of the transformed forward
         system and the multiplier');

% Bode plot of the system appearing in the stability condition
figure(10); clg;
  [a,b,c,d] = unpck(sys);
  [n,d] = ss2tf(a,b,c,d);
  bode(n,d,logspace(-2,4));
  subplot(2,1,1);
  title('Bode plot of the product of the transformed forward
         system and the multiplier');
```

Example3b.m

```
% Example 3
% Multiplicative uncertainty

clear all;

% System transfer function Gp(s)
num = 1;
den = conv(conv([1 1],[1 1]),[1 10]);

% PI Controller
k     = 120.8;   %109.07;
Ti    = 1.1426;
num_c = k*[Ti 1];
den_c = [Ti 0];
```

```
% Filter W(s) for Anti-Windup
T = 1;
num_f = 1;
den_f = [T 0];

% Filter W_D(s) of the multiplicative uncertainty
z = 10;
p = 1000;
num_fd = [1 z];
den_fd = [1 p];

% System G(s) used in the final loop
num_G11 = addpoly(Ti*conv([1 2 1],[1 10]), -T*k*[Ti 1]);
den_G11 = Ti*conv(conv([T 1],[1 10]),[1 2 1]);
[A_11,B_11,C_11,D_11] = tf2ss(num_G11,den_G11);
G_11 = pck(A_11,B_11,C_11,D_11);

num_G12 = -k*T*[Ti 1];
den_G12 = Ti*[T 1];
[A_12,B_12,C_12,D_12] = tf2ss(num_G12,den_G12);
G_12 = pck(A_12,B_12,C_12,D_12);

num_G21 = [1 z];
den_G21 = conv([1 p],conv([1 2 1],[1 10]));
[A_21,B_21,C_21,D_21] = tf2ss(num_G21,den_G21);
G_21 = pck(A_21,B_21,C_21,D_21);

num_G22 = 0;
den_G22 = 1;
[A_22,B_22,C_22,D_22] = tf2ss(num_G22,den_G22);
G_22 = pck(A_22,B_22,C_22,D_22);

G = sbs(abv(G_11,G_21),abv(G_12,G_22));
[G,sig] = sysbal(G);

% Slope bounds for the saturation
a = 0;
b = 1;

% Find the appropriate multiplier for the saturation
multiplier= [0 10];

% Find the appropriate multiplier for the uncertainty
R         = ritz(0.1,1,2);

IQC_Delta = Complexpar(R);
IQC_f     = slopeNL(multiplier,0,1);

% Augmentation of the descriptions of the two perturbations
```

```
IQC       = IQCdaug(IQC_f, IQC_Delta);

[Mstruc tmin] = IQCfeas(G,IQC,'FDIO',logspace(-2,2))
grid;
```

mult_plot.m

```
% This function finds the multiplier that is appearing
% in the stability condition and returns its Bode and
% Nyquist plots.

function multiplier=mult_plot(Mstruc,mult);

% Find the multiplier from the elements of Mstruc
r = size(Mstruc,1);
c = size(Mstruc,2);
d = Mstruc(1,r/2+1);
N = ((r/2)-1)/2;      % Number of basis multipliers
for i = 1:N
    % x(i)=(x+)-(x-) for i=1:N
    x(i) = Mstruc(2*i,r/2+2*i)-Mstruc(2*i+1,r/2+2*i+1)
    x(i) = x(i);
end

c = size(mult,2);
j=0;
for i = 1:2:c-1
    j = j+1;
    k(j) = mult(i);
    l(j) = mult(i+1);
end

% Use the conjugate of the multiplier for the stability condition
multiplier = d;
for i=1:N
    k_fact = 1;
    den_m  = [1 -l(i)];   % Denominator of the multiplier
    den_cm = [-1 -l(i)];  % Denominator of the conjugate of the multiplier
    for j=1:k(i)
        k_fact = k_fact*j;
        den_m  = conv(den_m,[1 -l(i)]);
        den_cm = conv(den_cm,[-1 -l(i)]);
    end;
    num_cm = k_fact;

    [a_cm,b_cm,c_cm,d_cm] = tf2ss(num_cm,den_cm);
```

```
    h_cm = pck(a_cm,b_cm,c_cm,d_cm);
    % Multiplier=d + Sum[x(i)*h(i)]
    multiplier = madd(multiplier,mmult(h_cm,x(i)));
end;

% Bode plot of the multiplier appearing in the stability condition
figure(5); clg;
  [a_mult,b_mult,c_mult,d_mult] = unpck(multiplier);
  [num_mult,den_mult] = ss2tf(a_mult,b_mult,c_mult,d_mult);
  bode(num_mult,den_mult,logspace(-2,4,1000));
  subplot(2,1,1);
  title('Bode plot of the multiplier');

% Nyquist plot of the multiplier
figure(6); clg;
  frs_mult=frsp(multiplier,logspace(-2,4,1000));
  vplot('nyq',frs_mult);
  grid;
  title('Nyquist plot of the multiplier');
```

Bibliography

[1] B. Armstrong-Hélouvry, P. Dupont, and C. Canudas de Wit. A survey of models, analysis tools and compensation methods for the control of machines with friction. *Automatica*, 30(7):1083–1138, 1994.

[2] Brian Armstrong-Hélouvry. *Control of Machines with Friction.* Kluwer Academic Publishers, 1991.

[3] ASME. *Nonlinear System Analysis and Synthesis*, volume 2 - Techniques and Applications. The American Society of Mechanical Engineers, 1980.

[4] Karl J. Åström and Björn Wittenmark. *Computer-Controlled Systems.* Prentice-Hall, 2 edition, 1990.

[5] Xin Chen and John T. Wen. Multiplier based stability analysis for LTI systems with structured incrementally sector bounded feedback nonlinearities. Preprint.

[6] H.B.Pacejka. *Tyre models for vehicle dynamics analysis*, chapter The magic formula tyre model, pages 1–6. SWETS & ZEITLINGER, 1993.

[7] Ulf Jönsson and Anders Rantzer. A format for multiplier optimization. Technical Report TFRT–7530–SE, Department of Automatic Control, Lund Institute of Technology, March 1995.

[8] A. Megretski and A.Rantzer. System analysis via integral quadratic constraints, part i. Technical Report TFRT–7531–SE, Department of Automatic Control, Lund Institute of Technology, 1995.

[9] P.Gahinet and A.Nemirovskii. *LMI-lab: A Package for Manipulating and Solving LMI's*, version 2.0 edition, 1993.

[10] A. Rantzer and A. Megretski. System analysis via integral quadratic constraints. In *CDC*, Florida, December 1994.

[11] Lars Rundqwist. *Anti-Reset Windup for PID Controllers.* PhD thesis, Department of Automatic Control, Lund Institute of Technology, 1991.

[12] Jean-Jacques E. Slotine and Weiping Li. *Applied Nonlinear Control.* Prentice-Hall International Editions, 1991.

[13] John T. Wen and Xin Chen. The optimal multiplier method for nonlinear robustness analysis. In *Proc. of American Control Conference*, pages 645–650, San Diego, CA, June 1990.

[14] J. C. Willems. Least squares stationary optimal control and the algebraic riccati equation. *IEEE Transactions on Automatic Control*, AC-16(6):621–634, 1971.

[15] G. Zames. On the input-output stability of nonlinear time-varying feedback systems - part i: Conditions derived using concepts of loop gain. *IEEE Transactions on Automatic Control*, 1(11):228–238, April 1966.

[16] G. Zames and P. L. Falb. Stability conditions for systems with monotone and slope-restricted nonlinearities. *SIAM J. Control*, 6(1):89–108, 1968.